Research article

JGS
Journal of the Geological Society

https://doi.org/10.1144/jgs2024-009 | Vol. 181 | 2024 | jgs2024-009

The application of chemostratigraphy and proximality trends to the Silurian Coralliferous Formation of SW Wales: rhythmical sedimentation during the transgression of a palaeo-shoreline

Sarah J. Veevers[1], David C. Ray[1]*, Kenneth T. Ratcliffe[2] and Alan T. Thomas[1]

[1] School of Geography, Earth and Environmental Sciences, University of Birmingham, Birmingham B15 2TT, UK
[2] Hollymount, Welshpool SY21 9BW, UK
* Correspondence: d.c.ray@bham.ac.uk

Abstract: The Silurian Coralliferous Formation of Pembrokeshire comprises 94–143 m of shelfal sediments deposited on the southern margin of the Welsh Basin, UK. The succession begins with rudites (Renney Slip Member), which are overlain by interbedded silty mudstone and sandstone (Deadman's Bay Member). Biostratigraphical control is weak between the two principal sections (Renney Slip and Marloes Sands), but high-resolution chemostratigraphy permits 11 subdivisions to be distinguished. Some chemostratigraphical units can be traced between the sections, whereas others are locally absent. The correlation of the chemostratigraphical units has been compared with sea-level cycles identified by a study of the frequency, distribution and characteristics of storm-beds using proximality trend analysis. This suggests a synchroneity of traceable chemostratigraphical units within the Deadman's Bay Member, indicating that deposition began in the Renney Slip Section, and that a greater water depth was achieved there. A holistic assessment shows that the Coralliferous Formation onlaps an unconformity surface with a palaeo-relief of 57 m, over a current distance of 3 km. Further considerations of benthic assemblages, subsidence rates and global sea-level fluctuations support the presence of a late Telychian transgression with glacio-eustasy contributing between 40 and 70 m to that sea-level rise.

Supplementary material: Key element and compound ratios plotted against thickness and discriminant analysis results are available at https://doi.org/10.6084/m9.figshare.c.7251814

Received 21 January 2024; **revised** 10 May 2024; **accepted** 14 May 2024

Studies of shallow-marine clastic sediments that onlap topographic relief on an unconformity surface in a rocky-shore environment are rarely reported in the rock record (Johnson 1992, 2023; Sheppard 2007; Puig López *et al.* 2023) and are frequently hampered by limited stratigraphic control. Such successions, if stratigraphically well constrained, can provide an accurate measure of sea-level change (i.e. a measure of the topographic relief of the unconformity surface buried by marine deposits in an intertidal setting), and help distinguish between a sea-level rise controlled by global processes involved in eustasy and local tectonic subsidence (Johnson *et al.* 1998). Furthermore, if the eustatic component of sea-level change can be sufficiently isolated from local processes, the duration and magnitude of sea-level cycles can be used to establish the likely drivers of orbitally forced and climate-linked eustasy (Simmons *et al.* 2020).

We present a study of two closely spaced (3 km apart) and well-exposed coastal sections through the Coralliferous Formation (Telychian, Silurian) of SW Wales, which allow for the identification of an unconformity surface with a topographic relief of 57 m and of sea-level cycles driven by glacio-eustasy. We show that the limited biostratigraphic control can be improved by chemostratigraphic techniques (Craigie 2018; Ray *et al.* 2021; Shields *et al.* 2022) that focus upon whole-rock elemental analysis (Ratcliffe *et al.* 2006, 2010, 2012, 2015), and by proximality trend analysis (Aigner and Reineck 1982; Aigner 1985; Seilacher and Aigner 1991) that focuses on water-depth-related sedimentary features to identify sea-level cycles (Easthouse and Driese 1988; Baarli 1998; Dahlqvist 2004). The resultant high-resolution stratigraphic framework, in combination with sedimentological, palaeoenvironmental and sequence stratigraphic analysis, has allowed for the creation of a depositional model and identified medium- and short-term sea-level cycles. The magnitude of these sea-level cycles was determined by the relief of the buried unconformity, alongside water depth estimates derived from benthic assemblage zones (Brett *et al.* 1993; Johnson 2006), as well as proximality trend analysis. Having established a relative sea-level curve, we show how sea-level cycles, in combination with limited biostratigraphy, may be linked to a sea-level curve that attempts to depict eustasy, and in doing so, not only suggests a eustatic driver of sea-level change, but provides an age model for the succession. The establishment of an age model allows the duration of sea-level cycles to be estimated, and the amount of tectonic subsidence (as derived from published regional subsidence curves) to be removed from relative sea-level changes, thereby allowing the eustatic components of sea-level change (duration and magnitude) to be better isolated.

Our study of the duration and magnitude of the sea-level cycles within the Coralliferous Formation is supportive of orbitally driven glacio-eustasy, with the identification of a globally expressed medium-term late Telychian sea-level rise with an estimated magnitude of 55 m (40–70 m range) requiring the melting of an ice sheet with a volume approximately equivalent to the present-day East Antarctica ice sheet. These findings highlight the importance of this succession as an example of Telychian global change, and support the notion of the waxing and waning of ice sheets as an important contributor to Silurian sea-level (Caputo 1998; Loydell 1998; Johnson 2006; Page *et al.* 2007).

Geological overview

Geological setting

The southern Pembrokeshire peninsula of SW Wales (Fig. 1) includes the most southwesterly Silurian rocks exposed in mainland Britain, and these were deposited on the southern (Pretannian)

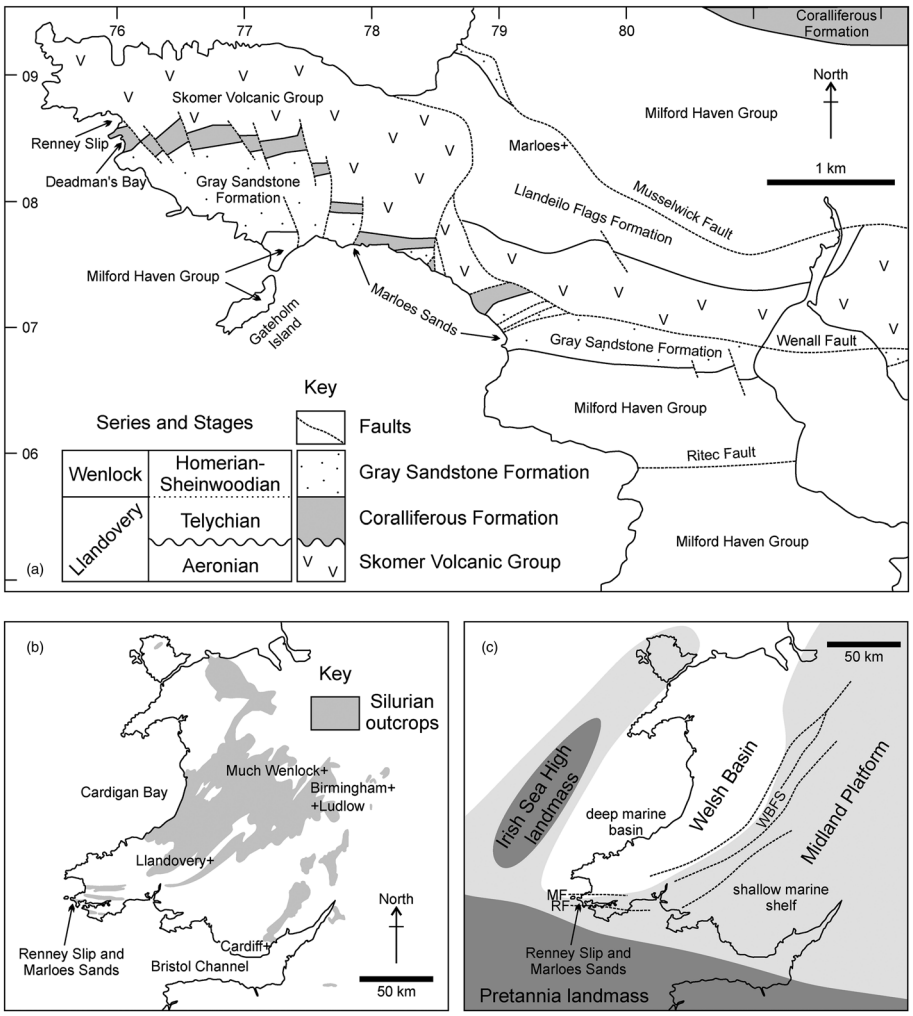

Fig. 1. Geological maps and regional setting of SW Pembrokeshire. (**a**) Geological sketch map showing the positions of the principal localities, structures referred to in the text and chronostratigraphy of key lithostratigraphic units. (**b**) Silurian outcrops in Wales and the Welsh Borderlands, highlighting the location of the study area and the type-Silurian successions around Llandovery, Much Wenlock and Ludlow. (**c**) A generalized Telychian palaeogeography of Wales and the Welsh Borderlands, showing the key structural and depositional features mentioned in the text. MF, Musselwick Fault; RF, Ritec Fault; WBFS, Welsh Borderland Fault System. Source: (a) contains British Geological Survey materials © UKRI (2024).

margin of the Welsh Basin. South Pembrokeshire was strongly affected by Variscan deformation, with crustal shortening estimated to be at least 26% (Dunne 1983), so the Silurian rocks now occur as inliers in the cores of anticlines related to the inversion of long-lived extensional faults (Dunne 1983; Powell 1987, 1989). The succession is most completely preserved in the Marloes Block, bounded by the Musselwick Fault to the north and the Ritec Fault to the south (Fig. 1a); there, a total Silurian thickness of some 3100 m is spectacularly exposed in coastal cliff sections. Like those of the Midland Platform to the east and NE, the Silurian rocks of SW Wales were deposited in a shelf to marginal marine setting. The Pembrokeshire succession contrasts in important respects, however: the Llandovery is thicker, more complete and dominated by volcanic rocks; the Wenlock and Ludlow lack prominent limestone formations; and the transition into Old Red Sandstone facies occurs earlier, approximately at the Wenlock–Ludlow boundary. Although less intensively studied than their Midland Platform equivalents, the Silurian succession of Pembrokeshire has a history of research extending back to Murchison (1839; for review see Veevers *et al.* 2007).

The Silurian rocks of the Marloes Block accumulated in the Skomer Sub-basin, one of a series of half-grabens formed in response to transtensional rifting (King 1994; Butler *et al.* 1997). The sub-basin is bounded by a series of inverted normal faults: the Wenall and Ritec faults in the immediate area, and the Musselwick and Benton faults a little further to the north (Fig. 1; Powell 1987, 1989; Hillier and Morrissey 2010, fig. 2b and c). Following accumulation of the Skomer Volcanic Group, there was an episode of local uplift in the late Aeronian and early Telychian (Walmsley and Bassett 1976; Clayton 1994) resulting in a short period of subaerial exposure (Hillier 2002) and an angular unconformity at the base of the overlying Coralliferous Formation (Siveter *et al.* 1989, fig. 99A, p. 104; Veevers *et al.* 2007, fig. 2, p. 320). Sedimentation recommenced with the deposition of a thin coarse-grained unit, the Renney Slip Member, at the base of the Coralliferous Formation (Hillier 2002; Veevers *et al.* 2007). Flooding then led to the deposition of the rhythmically bedded open-marine deposits of the overlying Deadman's Bay Member.

Lithostratigraphy

Three principal lithostratigraphical divisions make up the Silurian to Early Devonian succession in the Marloes Block. The oldest is the *c.* 1000 m thick Skomer Volcanic Group (Ziegler *et al.* 1969). Although dominated by volcanic rocks overall, the uppermost 150 m of the group is mainly sedimentary. Above, the Marloes Group (Hillier and Morrissey 2010) comprises an interval of predominantly shallow-marine clastic sedimentary rocks, separated by an unconformity from the Skomer Volcanic Group beneath, and distinct lithologically from the 1500 m thick Old Red Sandstone facies of the overlying Milford Haven Group (Allen and Williams 1978). Two formations ('groups' of earlier authors) are distinguished within the Marloes Group, the 94–143 m thick Coralliferous Formation (De La Beche 1846; Ziegler *et al.* 1969; Walmsley and Bassett 1976; Veevers *et al.* 2007) below and the <500 m thick Gray Sandstone Formation (see Hillier and Morrissey 2010) above. The lowest 6–12 m of the Coralliferous Formation comprise granule- to pebble-grade rudite beds of the Renney Slip Member, interpreted as fluvial and a wave-dominated shoreface (Hillier 2002) or fan-delta (Veevers *et al.* 2007) deposits. A prominent flooding surface

separates the Renney Slip Member from the overlying interbedded mudstones, sandstones and bioclastic limestones of the Deadman's Bay Member. These form a succession that passes conformably upwards into the Gray Sandstone Formation (Fig. 2).

The type sections of both members of the Coralliferous Formation (Veevers *et al.* 2007, p. 321) occur in the cliffs between Renney Slip [SM 7604 0864] and Deadman's Bay [SM 7602 0841]. For brevity in the following account, these sections are referred to simply as the Renney Slip Section. A second well-exposed section considered here is at Marloes Bay [SM 7872 0724 to SM 7878 0711], which we refer to as the Marloes Sands Section. Exposure of the Coralliferous Formation elsewhere in South Pembrokeshire is now limited (Veevers *et al.* 2007, p. 321).

Biostratigraphy

The macrofossil and microfossil content of the Coralliferous Formation provides good evidence for age at the stage level, but not for the high-confidence placement of stage or series boundaries or for the internal subdivision and correlation of lithostratigraphic units. Here we provide a summary of key biostratigraphic determinations that constrain the age of the Coralliferous Formation. In addition, the approximate positions of the boundaries between the faunas (II, III and IV) of Walmsley and Bassett (1976) are given, as are benthic assemblage (BA) zones (Fig. 2). The links between the faunas, benthic assemblage zones and water depth are discussed below (see 'The record of sea-level change in the Coralliferous Formation').

The base of the Skomer Volcanic Group is not seen, and its older parts yield no age-diagnostic fossils. Brachiopods occur towards the top of the succession (Thomas 1911; Ziegler *et al.* 1969; Walmsley and Bassett 1976), and these include *Eocoelia hemisphaerica* in the uppermost Skomer Volcanic Group at Renney Slip, indicating an Aeronian age for the rocks there (Fauna I of Walmsley and Bassett 1976). This age has been confirmed by a conodont assemblage, characterized by *Pranognathus tenuis*, from the same part of the succession (Aldridge *et al.* 2000, p. 98; 2002). There is an angular unconformity between this group and the overlying Renney Slip Member of the Coralliferous Formation that omits much of the Telychian and potentially part of the Aeronian.

No age-diagnostic body fossils occur in the Renney Slip Member, but brachiopods from the overlying Deadman's Bay Member (*Eocoelia sulcata* and *Costistricklandia lirata lirata*), alongside the solitary rugose coral *Palaeocyclus porpita*, are considered characteristic of the Telychian C_6 time interval, although they are known to range into early Sheinwoodian strata (Ziegler *et al.* 1968; Walmsley and Bassett 1976; Hurst *et al.* 1978; Bassett and Rong 2002; Scrutton and Deng 2002). The C_6 time interval is considered to begin at the base of the *crenulata* graptolite biozone and spans the remainder of the Telychian (Bassett and Rong 2002; Rickards and Chen 2002; Zalasiewicz *et al.* 2009). Furthermore, it is the youngest of three brachiopod-defined Telychian time intervals (i.e. C_4, C_5, C_6), which approximate to the early, middle and late Telychian. Additionally, within the upper quarter of the Deadman's Bay Member in the Renney Slip Section, the replacement of *Eocoelia sulcata* by *Eocoelia angelini* is suggestive of the transition between the Telychian and Sheinwoodian (Walmsley and Bassett 1976; Bassett and Rong 2002). Within the overlying lower parts of the Gray Sandstone Formation the marine shelly fauna is characterized by the disappearance of *Eocoelia* and the dominance of a *Salopina conservatrix* and bivalve community that is considered more likely to be of Wenlock than of Llandovery age

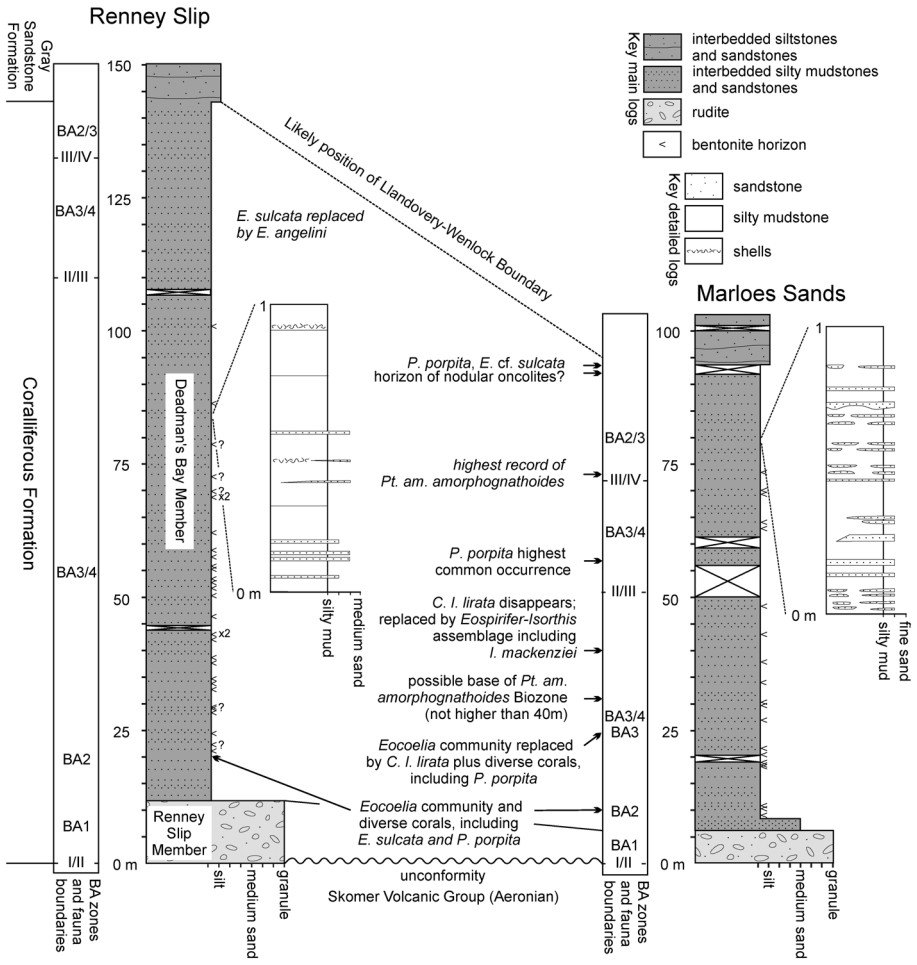

Fig. 2. Summary sedimentary logs illustrating the total thickness of the Coralliferous Formation in its two principal sections, alongside key biostratigraphic occurrences, benthic assemblage (BA) zones and faunal boundaries (II–III, III–IV) referred to in the text. Inset logs to the right of these show detailed variations in lithology. It should be noted that biostratigraphic occurrences, faunal boundaries and benthic assemblage zones represent approximate stratigraphic positions derived from the collation of information from multiple sources, which sometimes conflict in detail. Sources: Walmsley and Bassett (1976), Hurst *et al.* (1978), Mabillard and Aldridge (1983) and Aldridge *et al.* (2002).

(Hurst *et al.* 1978), although marked shallowing may have exerted a strong facies control on the benthic communities. Accordingly, macrofossil records indicate a probable late Telychian age for the bulk of the Coralliferous Formation. This age assignment is supported by small numbers of the conodont *Pterospathodus amorphognathoides* between 20 and 73 m above the base of the Coralliferous Formation at Marloes Sands (Mabillard and Aldridge 1983, table 1, p. 31). The systematics and biostratigraphical distribution of *Pt. amorphognathoides* and its allies have since been revised (Männik and Aldridge 1989; Männik 2007). P. Männik has restudied the available material from Mabillard and Aldridges' study and reported (pers. comm. 2015) that *Pt. amorphognathoides amorphognathoides* certainly occurs in the higher parts of the succession and that the base of its zone lies not more than 40 m above the base of the formation, probably below 31 m, and possibly lower than that. The *Pt. am. amorphognathoides* conodont zone spans a significant part of the late Telychian and the Llandovery–Wenlock boundary (Cramer *et al.* 2011; Melchin *et al.* 2020), and its occurrence is a key age marker within the Coralliferous Formation.

Both macrofossil and conodont records indicate a late Telychian age for most of the Coralliferous Formation. However, the position of the Llandovery–Wenlock boundary is uncertain, and on biostratigraphic grounds may occur within the higher parts of the Coralliferous Formation through to the lower parts of the Gray Sandstone Formation. For example, the Llandovery–Wenlock boundary has been placed halfway through the Deadman's Bay Member within the upper half of Fauna II (Walmsley and Bassett 1976) and immediately beneath the Gray Sandstone Formation (Hurst *et al.* 1978; Aldridge *et al.* 2002). Comparisons between the positions of lithostratigraphic boundaries relative to the Llandovery–Wenlock boundary across the Midland Platform and Welsh Basin reveal a widespread close proximity (Cocks *et al.* 1992; Aldridge *et al.* 2002), suggesting that the Llandovery–Wenlock boundary corresponds to a regionally expressed change in sedimentation, as is also the case for the Wenlock–Ludlow boundary. Accordingly, a synchronicity between the Coralliferous–Gray Sandstone formation boundary and the Llandovery–Wenlock boundary seems likely.

Chemostratigraphy and high-resolution correlation of the Coralliferous Formation

The available biostratigraphical data are insufficient for the detailed subdivision of the Coralliferous Formation. Chemostratigraphy, utilizing variations in the geochemical characteristics of sedimentary successions to characterize geochemical units, offers the potential for more refined correlation; its use in the correlation of siliciclastic successions is well documented (e.g. Ratcliffe *et al.* 2006; Ray *et al.* 2021; Shields *et al.* 2022; and references therein). The geochemical variations can reflect a range of factors including changes in lithology and sediment provenance, climatic shifts in the hinterland, redox conditions in the basin and changes in diagenetic history. Ratios of elements and compounds are used to define stratigraphical divisions within the sedimentary succession that we term 'packages', which each show distinctive geochemical signatures. More subtle geochemical patterns within packages are used to distinguish geochemical 'units'. Because of the large number of variables that can influence geochemical variations, interpretations based on single samples should be viewed with caution; rather they should be based on patterns and trends that incorporate numerous samples. Therefore, within a particular unit, not every sample will necessarily fit the overall geochemical signature of that unit neatly. Accordingly, individual data points need to be considered in the context of the dataset overall, and sample outliers may occasionally need to be disregarded.

For this study, data for 47 elements and compounds were determined using X-ray fluorescence (XRF), supported by inductively coupled plasma optical emission spectrometry (ICP-OES) and inductively coupled plasma mass spectrometry (ICP-MS), as shown in Table 1. The ICP–OES and ICP–MS samples were prepared and analysed using the techniques described by Jarvis and Jarvis (1992) and Pearce *et al.* (1999, 2005). The XRF samples were prepared by removing surface contamination and mechanically grinding each rock sample to form a powder. This was pressed into a 28 mm diameter wafer, and then analysed on a Bruker-AXS S4 Explorer wavelength-dispersive XRF spectrometer.

Samples were collected at approximately 1 m intervals from both sections, yielding a total of 220 samples for analysis. Sampling from a single rock-type minimizes variations that simply reflect overall lithology, and mudstone was selected because the settling of fine-grained suspended material during deposition tends to preserve consistent geochemical signatures over relatively wide geographical areas. Absolute element and compound concentrations were plotted relative to stratigraphical position to produce chemical logs for the two sections: components that appeared to show systematic changes through time were then selected as key chemostratigraphical markers. For the Coralliferous Formation these are Al_2O_3 (reflecting total clay content), SiO_2 (a proxy for total silt or sand content), MgO (high values are probably mostly carbonate-related but, where carbonate values are low, MgO is influenced strongly by chlorite distribution), Na_2O (strongly influenced by plagioclase feldspar content), K_2O and Rb (strongly influenced by K-feldspar and illite content), TiO_2 and Nb (both related to heavy minerals such as rutile, with a possible contribution from volcanogenic material) and Zr (related to zircon). Ratios of these elements and compounds were calculated to highlight and emphasize subtle changes in the absolute values.

Figure 3 shows the geochemical signatures for major rock-forming components (Al_2O_3, SiO_2 and CaO) and a proposed subdivision of the Coralliferous Formation into packages and their more subtle subdivision, units (see below). Excepting the occasional enrichment or depletion, these show relatively little general variation, indicating that the geochemical changes within the Coralliferous Formation documented below do not simply reflect variations in sand–silt–clay–carbonate content. An exception does occur at the top of the succession, where Package D shows a rise in SiO_2 and a decrease in Al_2O_3, representing a small increase in the proportion of silt and fine sand to clay, and reflects the transition to the sand-rich Gray Sandstone Formation. Similarly, the plot for CaO is rather spiky at Marloes Sands, probably reflecting the sporadic occurrence of calcareous shell fragments in some samples,

Table 1. Summary of the geochemical data analysed for this study and the analytical techniques employed

Technique	Major elements (as oxides)	Trace elements	Rare earth elements
XRF	Al_2O_3, SiO_2, TiO_2, Fe_2O_3, MnO, CaO, MgO, K_2O, Na_2O and P_2O_5	Ba, Cl, Co, Cr, Cs, Cu, Ga, Hf, Mo, Ni, Nb, P, Rb, S, Sc, Sr, Ta, Th, U, V, Y, Zn and Zr	La, Ce and Yb
ICP-OES and ICP-MS	As above	As above plus Be and Sn	As above plus Nd, Pr, Sm, Eu, Gd, Tb, Tm, Dy, Ho, Er and Lu

XRF, X-ray fluorescence; ICP-OES, inductively coupled plasma optical emission spectrometry; ICP-MS, inductively coupled plasma mass spectrometry.

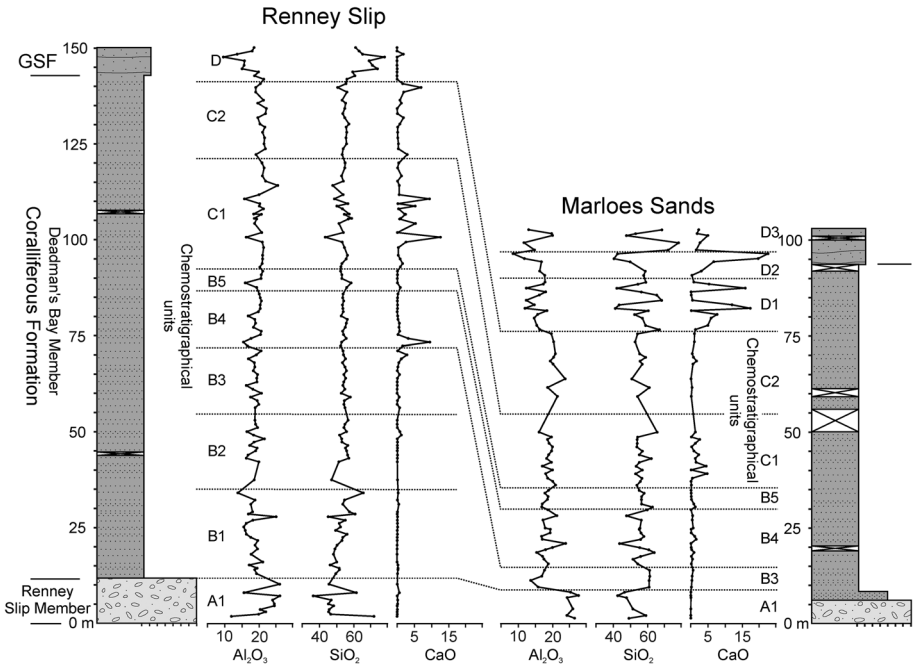

Fig. 3. Plots showing stratigraphical variations in Al_2O_3, SiO_2 and CaO in the Renney Slip and Marloes Sands sections; these oxides are respectively proxies for the amounts of clay, silt–sand and carbonate in the succession. Four chemostratigraphical packages are distinguished, denoted packages A–D; packages B–D are subdivided into smaller units (B1, B2, etc.). GSF, Gray Sandstone Formation.

as the succession becomes richly fossiliferous and associated with carbonate beds.

Chemostratigraphical correlation and subdivision of the Coralliferous Formation has been based upon chemical logs for selected key ratios that pick out the packages and units (Fig. 3 and Supplementary material 1 and 2). Each chemostratigraphical package has a chemical signature different from others in the interval (Table 2). In ascending stratigraphical order, the packages are designated by the letters A–D; packages B–D are subdivided into units, denoted by B1, B2, etc. The subdivision of packages into units is based on key geochemical features as summarized in Tables 3 and 4: the units have a geochemical signature different from others in their parent package, but not necessarily different from others in the entire succession.

The robustness of the chemostratigraphical packages identified was tested by plotting key ratios against each other: if the packages are robust, bivariate plots should show clear groupings of the data for each package. Figure 4 summarizes the chemostratigraphical distinction between the two members of the Coralliferous Formation and the packages identified within the Deadman's Bay Member. Discriminant function analysis was used to test the proposed correlation: the analysis was performed using Unistat for Windows and all analysed components were input as variables; multiple canonical discriminant analysis options were selected. The results (summarized in Supplementary material 3) show that 98.45% of the data points were correctly classified, a high degree of concurrence between correlations proposed on chemical log and graphical analysis and multivariate statistical analysis. The remaining 1.55% of samples most probably represent anomalous enrichments and depletions.

Based upon the identification of robust chemostratigraphical packages and their subdivision into units, a more refined subdivision of the Coralliferous Formation has been achieved. Package A occurs in both sections and is equivalent to the Renney Slip Member, as well as the lowest 2.2 m of the Deadman's Bay Member at Marloes Sands. Three packages (B–D) are recognized within the Deadman's Bay Member. Package B is recognized in both sections, and embraces five units, with B1 and B2 present only in the Renney Slip section; the top part of Unit B3 is present at Marloes Sands. Furthermore, Package B, at the base of the Deadman's Bay Member, is 50.26 m thicker in the Renney Slip section, reflecting the presence of the units that occur only there (Fig. 3 and Supplementary material 1 and 2). Such an arrangement indicates a significant local hiatus at the Marloes Sands Section, above which the thicknesses of the units that make-up the remainder of Package B and Package C are similar, thereby indicating a uniformity of sedimentation rates. An additional contrast is identified within Package D, which occupies a significantly greater thickness and can be divided into units D1, D2 and D3 at Marloes Sands. In this instance, it is unclear at Renney Slip whether this reflects the occurrence of the units in the unsampled and overlying parts of the Gray Sandstone Formation, the absence of one

Table 2. Key geochemical features and their interpretation for each chemostratigraphical package

Package	Main geochemical features	Interpretation
D	Low TiO_2/Zr	High zircon:rutile ratio
	High Zr/Nb	
C	High Rb/Al_2O_3	High K-feldspar and illite
	Moderate Fe_2O_3/MgO	Intermediate chlorite
	Low Zr/Nb	Low zircon:rutile ratio
B	Low Fe_2O_3/MgO	High chlorite
	High Na_2O/Nb	High plagioclase:rutile ratio
	High Na_2O/K_2O	High plagioclase or K-feldspar and ?illite
A	High Rb/Al_2O_3	Clay mineral related; probably more illitic

The terms 'high' and 'low' refer to the relative values between packages.

Table 3. Key geochemical features and their interpretation for each chemostratigraphical unit

Unit	Main geochemical features	Interpretation
D3	High Zr/Nb	High zircon:rutile ratio
	Low TiO_2/Zr	
D2	Moderate TiO_2/Zr	Moderate zircon:rutile ratio
	Low Na_2O/Nb	Low plagioclase:rutile ratio
	Low Na_2O/K_2O	Low plagioclase:K-feldspar ratio
	High Rb/Al_2O_3	Possibly high illite
D1	Low Na_2O/Nb	Low plagioclase:rutile ratio
	Low Na_2O/K_2O	Low plagioclase:K-feldspar ratio
C2	High Rb/K_2O	Influenced by clay minerals (illite) and K-feldspar
	Moderate Fe_2O_3/MgO	Influenced by chlorite
C1	High Rb/K_2O	K-feldspar
	Moderate TiO_2/Nb	Change in provenance, possible volcanic input
	Low Zr/Nb	Low zircon:rutile ratio
B5	High TiO_2/Nb	Heavy minerals
B4	High TiO_2/Nb	High heavy minerals
	High Rb/K_2O	High K-feldspar
	Low Zr/Nb	
B3	High TiO_2/Nb	High zircon:rutile ratio
	Low Fe_2O_3/MgO	High chlorite
	Moderate Na_2O/Nb	
B2	Low Fe_2O_3/MgO	High chlorite
	High Na_2O/Nb and Na_2O/K_2O	High plagioclase:rutile ratio
B1	High Fe_2O_3/MgO	Low chlorite
	High TiO_2/Nb	Influenced by heavy minerals or volcanic rocks
A	Low Na_2O/Nb	Low plagioclase:rutile ratio
	High Rb/Al_2O_3	Clay minerals

The terms 'high' and 'low' again refer to comparisons between units.

or more units, or a thinning of Package D so to preclude the identification of units.

Sedimentology, palaeoenvironments and proximality trends

Sedimentology of the Coralliferous Formation

Having established a chemostratigraphic framework for the Coralliferous Formation the synchronicity of the chemostratigraphical packages and units has been assessed by a detailed investigation of the sedimentology, palaeoenvironments and proximality trends. In particular, we compare the chemostratigraphic framework with short-term sea-level cycles, which are potentially traceable and time synchronous events.

The two coastal sections exposing the Coralliferous Formation were logged on a scale of 1:10, as summarized in Figure 2. The sedimentology of the Renney Slip Member has been previously described in detail (Hillier 2002; Veevers *et al.* 2007) and our brief description of the Renney Slip Member here is aimed at providing additional context for the overlying Deadman's Bay Member.

The Renney Slip Member consists of rudites, sandstones and silty mudstones, which can be separated into three alternating and locally cyclic lithofacies (Veevers *et al.* 2007). Beds are up to 0.94 m thick and display a range of structures including rippled bed tops, parallel lamination, cross-stratification and hummocky cross-stratification.

Table 4. Summary of key geochemical characteristics used to recognize the chemostratigraphical unit boundaries, and their interpretations

Boundary	Main geochemical features	Interpretation
Base D3	Increase in SiO_2/Al_2O_3, Zr/Nb and TiO_2/Nb	Change in detrital mineralogy or provenance
	Decrease in TiO_2/Zr	
Base D2	Decrease in Na_2O/Nb, NaO_2/K_2O and Rb/K_2O	Decrease in plagioclase and K-feldspar
Base D1	Increase in SiO_2/Al_2O_3 and Zr/Nb	Becoming siltier
	Decrease in TiO_2/Zr	Change in detrital mineralogy or provenance
Base C2	Decrease in Na_2O/Nb and NaO_2/K_2O	Decrease in plagioclase
	Increase in Fe_2O_3/MgO	Decrease in chlorite or clay minerals
Base C1	Increase in Rb/K_2O, TiO_2/Zr and Fe_2O_3/MgO	Change in clay mineralogy, feldspar and heavy mineral content
Base B5	Increase in Rb/K_2O, Rb/Al_2O_3 and Fe_2O_3/MgO	Change in clay mineralogy
Base B4	Increase in TiO_2/Zr and Rb/K_2O	Upward increase in K-feldspar
	Decrease in Na_2O/Nb and NaO_2/K_2O	
Base B3	Slight increase in Fe_2O_3/MgO	Change in detrital mineralogy or provenance and change in chlorite content
	Decrease in Zr/Nb	
Base B2	Decrease in Na_2O/Nb and NaO_2/K_2O	Change in detrital component (feldspar) and change in chlorite content
	Decrease in Fe_2O_3/MgO	
Base B1	Decrease in Zr/Nb	Change in detrital mineralogy or provenance
	Increase in Na_2O/Nb and NaO_2/K_2O	

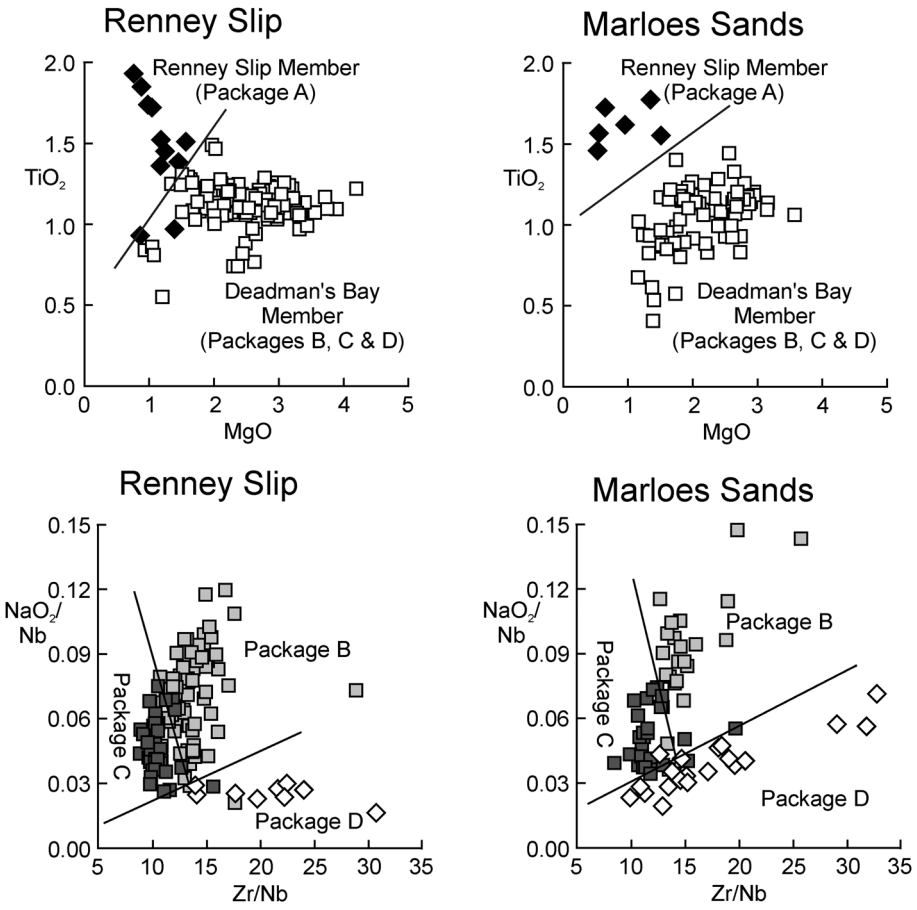

Fig. 4. The chemostratigraphical distinction between the two members of the Coralliferous Formation and the packages identified within the Deadman's Bay Member at Renney Slip and Marloes Sands. (Top) Bivariate plots summarizing the chemostratigraphical distinction between the Renney Slip and Deadman's Bay members of the Coralliferous Formation. (Bottom) Bivariate plots of NaO_2/Nb and Zr/Nb ratios, illustrating the distinction of chemostratigraphical packages B, C and D.

The rudites are polymictic and especially rich in reddened acid volcanic and granodiorite clasts. Seven sedimentary cycles have been identified in the Renney Slip section, and four at Marloes, but these cannot be correlated with certainty between the sections (Hillier 2002; Veevers *et al.* 2007). The finer lithofacies of the Renney Slip Member contain glauconite, which occurs as isolated and agglutinated pellets up to 1 mm across, and sedimentary pyrite. Body fossils are restricted to disarticulated crinoid ossicles and shell fragments, including lingulid brachiopods, and bioturbation is evidenced by sand- or mud-filled vertical and horizontal burrows.

A prominent flooding surface marks the base of the Deadman's Bay Member at Renney Slip, with a sharp lithological change from rudaceous rocks below to interbedded mudstones and fine sandstones above. In the Marloes Sands section by contrast, the lowest 2.2 m of the member are dominated by sandstone beds up to 180 mm thick, which have erosive bases, shelly layers, cross-lamination and bed amalgamation. Except for this basal interval at Marloes Sands, the Deadman's Bay Member in both sections is dominated by silty mudstone with subordinate very fine- to fine-, occasionally medium-grained sandstone, shelly sandstone and rarer bioclastic limestone interbeds. The coarser beds are mainly sandstones and shelly sandstones in the lower part of the succession. There, the fossiliferous beds contain transported tabulate and solitary rugose corals, brachiopods (mostly strophomenids and pentamerids) and shell fragments. Some such beds have scattered shells at their bases, overlain by sand. The upper part of the succession contains a higher proportion of bioclastic material, and less sand: some contain whole solitary corals, others densely packed broken shells or disarticulated crinoid ossicles and nodular oncolites (Aldridge *et al.* 2002).

In detail, over 2000 sandy and shelly beds were identified in total in the two sections of the Deadman's Bay Member; most are 5–10 mm thick, with a maximum of 250 mm. Individual bed thickness varies laterally, and many are discontinuous at outcrop scale with an isolated ripple- or lens-like geometry. Beds are sharp-based, with some showing marked basal erosion. Internal sedimentary structures in the sandstones include normal grading, parallel- and cross-lamination and rare hummocky cross-stratification. Many beds have parallel lamination below, overlain by cross-lamination and a symmetrically or asymmetrically rippled gradational top. Finer sandstone beds can appear internally structureless in the field, but this is probably due to tectonism and weathering because lamination is visible in thin section. The average thickness of sandstone beds, and the sandstone:silty mudstone ratio, varies in the succession, as further discussed below.

Bioturbation associated with the sandstone beds is characteristically seen in the field as hypichnia on bed bases, with 10–15 mm diameter vertical burrows and 1–6 mm wide straight to branching horizontal ones. In thin section and on polished slabs, abundant bioturbation is seen at the tops of sandstone beds too. In the silty mudstones, 1–6 mm diameter sand-filled burrows are the most common, but detailed field study of burrows in this lithofacies is impossible because of the pervasive cleavage. Detailed study was therefore based on large blocks that could be cut and polished. The Bioturbation Index (BI) of Taylor and Goldring (1993) provides a measure of bioturbation intensity in relation to primary bedding features: grades are assigned based on burrow density, amount of burrow overlap and distinctness of the original sedimentary fabric, on a scale where zero equals no bioturbation, and six equals 100% bioturbated. Silty mudstone samples from parts of the succession containing the highest number of sandstone beds per metre had a BI of 1–2, and those from intervals with the fewest had BI 0–3. Samples from intermediate positions showed the highest values, BI 3–6.

A further feature of the Deadman's Bay Member is thin, pale green–grey to yellow–buff bentonites, representing degraded volcanic ash deposits: 31 in the Renney Slip section and 20 at Marloes Sands (Fig. 2). Thicknesses are variable, with maxima ranging from 10 to 300 mm. Grain size is dominantly clay-grade,

and these deposits are highly altered, with a bulk composition close to illite. On magmatic discrimination diagrams (Veevers 2006), the Deadman's Bay Member bentonites plot principally within the dacite–rhyodacite field, like other Silurian examples from the Welsh Basin (Huff *et al.* 1996; Ray 2007).

Palaeoenvironment of the Coralliferous Formation

The Renney Slip Member is interpreted here in the context of a fan delta depositional model (Veevers *et al.* 2007): the rudite beds (Lithofacies 1) represent a variety of mass-flow deposits, some of which have been reworked in a marine environment; thick sandstones with planar and ripple lamination (Lithofacies 2) are shoreface to offshore transition zone deposits; silty mudstones interbedded with very fine-grained sandstones (Lithofacies 3) represent marine offshore deposits, formed largely below mean storm wave-base. The presence of crinoid and lingulid brachiopod fragments, bioturbation, sedimentary pyrite and glauconite indicates an environment with a strong marine influence. An alternative interpretation has suggested the localized development of a fluvial environment within the basal 4.25 m of the Renney Slip section, followed by the more geographically extensive development of a marine shoreface environment (Hillier 2002; for discussion see Veevers *et al.* 2007). Common to both interpretations is the occurrence of small-scale cyclic packages of sedimentary rock that reflect short-term sea-level cycles developed during the onlap of dominantly proximal sediments across a subaerially exposed topography. Accordingly, the Renney Slip Member and its chemostratigraphical signature (Package A) can be viewed as a transgressive deposit linked to the initial flooding of the area and erosion of the basement, and as such is likely to be time-transgressive. Diachronism can also explain the difficulty of confidently correlating the short-term sedimentary packages between the Renney Slip and Marloes Sands sections: the cycles are not time-equivalent, and represent different episodes of deposition.

Our interpretation of the depositional setting of the Deadman's Bay Member accords broadly with those briefly outlined previously (Ziegler *et al.* 1969; Sanzen-Baker 1972; Walmsley and Bassett 1976; Hillier 2002), and is discussed in more detail in this section. Body fossils, bioturbation and the presence of sedimentary pyrite indicate an open-marine environment. The alternating lithologies that dominate the succession respectively represent deposition during quiet 'background' conditions (the silty mudstones) and higher energy, periodic events (the sandstones, shelly sandstones and bioclastic beds); variation in these lithologies are of use for establishing proximality trends and identifying potentially traceable short-term sea-level cycles. The lack of glauconite in the member suggests reasonably high rates of sedimentation, leaving no time for authigenic mineral formation. This contrasts with the glauconite-containing transgressive deposits of the Renney Slip Member, and probably reflects a switch to the aggradation and progradation of sediments as transgression gives way to a highstand systems tract. Primary sedimentary structures observed within the event beds are characteristic of those observed in modern and ancient storm deposits (e.g. Aigner and Reineck 1982; Aigner 1985; Baarli 1988; Seilacher and Aigner 1991; Dahlqvist 2004) and that feature in storm deposit facies models (e.g. Aigner and Reineck 1982; Aigner 1985; Pemberton *et al.* 2001). The sharp or erosive bed base represents the initial erosive capability of the storm, and this is overlain by the coarsest grained material, commonly a shelly lag, depending on the type of sediment available. The parallel and cross-lamination represent the oscillatory component of the storm waves or currents (Aigner 1985; Myrow and Southard 1996). Parallel lamination formed as the storm began to wane, but while turbulence was still sufficient to move water-saturated sheets of sand along the bottom. Cross-lamination formed later, under lower energy conditions (Seilacher and Aigner 1991). It is commonly thought that hummocky cross-stratification is solely a storm-generated structure. This stratification style is not environmentally specific, however (Rust and Gibling 1990; Mutti *et al.* 1996, table 2; Rees *et al.* 2014, p. 71), but records the interplay between oscillatory and unidirectional currents irrespective of whether the unidirectional component was storm-induced geostrophic flow or flood-generated hyperpycnal flow (Myrow *et al.* 2002; Lamb *et al.* 2008). The occurrence of hummocky cross-stratification in the Deadman's Bay Member is consistent with our palaeoenvironmental interpretation of the succession nevertheless. The characteristics of the 2.2 m thick sandstone-dominated interval at the base of the Deadman's Bay Member at Marloes Sands suggest shallower-water deposition in a shoreface setting, which gave way to a more typical open-marine environment above, and indicate continued transgression within the lower part of the Deadman's Bay Member. The sandier topmost Deadman's Bay Member and return of a shoreface setting within the overlying Gray Sandstone Formation indicate regression and the establishment of a highstand systems tract (Hillier 2002).

The event beds represent day- to week-long storm events (Kauffman *et al.* 1991) that brought coarser-grained sediment into the depositional environment. Both ancient and modern storm layers are discontinuous (Aigner 1985), patchy deposition on the topographically lowest parts of the seafloor reflecting limitations in sediment volume and lateral variation in the effects of a storm. An individual tempestite bed can extend only as far as the effects of the storm were felt, and down to effective wave-base (Seilacher and Aigner 1991). Once deposited, the sediment may then be redistributed or removed by later storms. Bioturbation indicates oxic bottom conditions (Dahlqvist 2004). Extensive horizontal traces with a different sediment fill but no lining are often produced by deposit feeders: these are common in lower energy environments because of limited suspended nutrient supply and a consequent lack of suspension feeders (e.g. Pemberton *et al.* 2001). Body fossil faunal composition is essentially uniform through a significant thickness of the Deadman's Bay Member. Shelly fossils are concentrated in the event beds and are largely absent from the muddy interbeds; fossils are commonly broken, but some shells remain articulated. These characteristics suggest an allochthonous fauna, but one that has not been transported over any great distance.

Whereas the distribution of storm-beds requires further discussion to assess their correlation and synchronicity, bentonites, a common feature of the Deadman's Bay Member, have the potential to act as time-lines (Ray 2007; Huff 2016; Ray *et al.* 2019, 2020). Individual bentonites should have been deposited across the whole of the small study area. However, the stratigraphic position and number of bentonites differs between the Renney Slip and Marloes Sands sections. In part, this probably reflects the local removal of bentonites by storm events. The absence of bentonites from the more proximal Renney Slip Member may be accounted for by a combination of penecontemporaneous erosion and an overall faster rate of deposition. Nevertheless, bentonites are notably more common and closely spaced in the lower part of the Deadman's Bay Member at Renney Slip, compared with the remainder of the overlying succession there and most of the member in the Marloes Sands section. Accordingly, the absence of a lower bentonite-rich part of the succession at Marloes Sands reflects the significant local hiatus at the base of the Deadman's Bay Member and the absence there of chemostratigraphic units B1, B2 and the lower part of unit B3.

Proximality trends and sedimentary cycles within the Coralliferous Formation

Studies of shallow-marine clastic sediments from modern onshore–offshore profiles show that systematic variations occur in such important characteristics as grain size, bed thickness, sedimentary

structures and degree of bioturbation; these are termed proximality trends (Aigner and Reineck 1982). The patterns observed reflect variations in a range of depth-related environmental factors that influence sediment deposition, notably environmental energy, the grain size of sediment being supplied and sedimentation rate. Most commonly, the proportion of sand, sandstone bed thickness and degree of amalgamation all decrease with increasing depth and distance from the shoreline (for discussion of exceptions see Myrow *et al.* 2002; Rees *et al.* 2014, p. 88), whereas the intensity of bioturbation generally rises. Proximality trend characteristics are readily preserved in the rock record, so detailed documentation of their stratigraphical variation in sedimentary successions can be used to infer changes in water depth over time (Aigner and Reineck 1982; Baarli 1988; Cotter 1988; Easthouse and Driese 1988; Dahlqvist 2004).

Visual inspection of the sedimentary logs of the Deadman's Bay Member suggests that some parts of the section contain more abundant but thinner event beds per unit thickness, whereas fewer and thicker event beds characterize other parts. The pattern was tested using the Kolmogorov–Smirnov test statistic, using the null hypothesis of an even distribution, and found to be significant at the 95% level. Having identified significant variation within an otherwise broadly uniform succession, the patterns were investigated further using proximality trend analysis (Aigner and Reineck 1982; Aigner 1985). This provides a method of analysing storm beds and cycles of deposition reflecting changes in water depth and distance from the shore. It can yield high-resolution palaeobathymetric data and so underpin the construction of detailed sea-level curves (Baarli 1998). The method requires centimetre-scale description of the sedimentary succession and statistical analysis of the frequency and thickness of event beds. Additional features such as the occurrence of cross-lamination, distribution of amalgamated beds and bioturbation were also investigated, but owing to sampling difficulties related to the presence of a pervasive cleavage, did not provide statistically meaningful data. Proximality trend analysis data for the Deadman's Bay Member are summarized in Figure 5.

Peaks and troughs in the proximality data reflect changes in water depth (Fig. 5). Broadly, maxima in event bed frequency, the percentage of event beds per metre, and maximum and mean event bed thickness reflect peaks in shallowing, whereas minima in the same metrics represent deepening. The serrated nature of the proximality data curves indicates that changes in water depth and the resultant variations in the position of wave-base relative to the seafloor can be detected over a range of scales, from a few metres to several tens of metres. Here we have attempted to identify sea-level changes that are traceable between the Renney Slip and Marloes Sands sections, as well as major events detected only in a single section. Generally, such events are expressed as pronounced shifts between peaks and troughs in the proximality data and contain lesser peaks and troughs that form part of an overall deepening or shallowing trend. To highlight these events, the proximality trend data have been shaded to indicate trends in sea-level change: dark grey represents the deepest water with flooding surfaces (fs1 to fs13) identifying their maxima, and white the shallowest, with light grey representing intermediate water depths (Fig. 5).

Comparisons between the sea-level highs and lows and the chemostratigraphical units within the Deadman's Bay Member confirm their synchronicity and correlation. Notably, seven sea-level highs (fs4 to fs10) and sea-level lows can be correlated, within their respective chemostratigraphical units, between the Renney Slip and Marloes Sands sections (Fig. 5). In addition, broad patterns such as a progressive decline in event bed frequency and variability, within chemostratigraphical units C1 and C2, are shared between the sections, whereas the sea-level changes identified within chemostratigraphical units B1 to lower B3 and D1 to D3 are observed only within a single section, the Renney Slip and Marloes Sands sections, respectively.

Apart from their use as a means of correlation, the proximality data highlight differences in the water depth between the sections. Notably, troughs in the proximality data, where values approach or reach zero, reflect deepening maxima to near the lower limit of storm sedimentation. These are evident only in the Renney Slip section, thereby identifying it as representing a more distal setting. Such an arrangement fits in with Renney Slip being the first section to be transgressed by the sea and accounts for the absence of chemostratigraphical units B1 to lower B3 at Marloes Sands. Troughs in the proximality data where values approach or reach zero at Renney Slip are restricted to four short-term flooding surfaces (fs3 to fs6) within the B3 and B4 chemostratigraphical units. Accordingly, it seems likely that following an initial phase of transgression (transgressive systems tract), a medium-term sea-level high (maximum flooding interval) occurs within the B3–B4 interval, the magnitude of which can be further refined using benthic assemblages (see below).

The record of sea-level change in the Coralliferous Formation

Palaeotopography of the unconformity surface at the base of the Coralliferous Formation

Based on the interpretation of chemostratigraphical units, sedimentology, palaeoenvironments and proximality trends, the Coralliferous Formation between the Renney Slip and Marloes Sands sections can be viewed as being deposited over an unconformity surface eroded into an elevated area of the Skomer Volcanic Group and other older rocks (Fig. 6). Variations in the relief of the unconformity surface can be estimated by differences in the thickness of the onlapping Coralliferous Formation, as sediment deposited upon an unconformity surface will accumulate first at the lowest point and will thin over any topographic high. Alternative interpretations, linked to differential subsidence and synsedimentary movement along faults, which could have acted to thicken the succession at Renney Slip without the need for a palaeotopography, are considered less likely owing to the uniformity of sediment thickness between the sections within chemostratigraphical units B4 to C2, which indicates tectonic stability for more than half the thickness of the Coralliferous Formation. The flattening and correlation of the Renney Slip and Marloes Sands sections using the chemostratigraphical B3–B4 unit boundary and its accompanying interval of short-term sea-level shallowing allows for differences in thickness of the Coralliferous Formation between this marker and the unconformity surface to be established and the palaeo-relief of the unconformity to be estimated. Based upon these considerations, the unconformity at Marloes Sands is 57 m above that at Renney Slip, and given a present-day distance of 3 km between the sections suggests only a modest gradient ratio (1:52) between the two. However, this does not allow for Variscan deformation and shortening (Dunne 1983), and accordingly should be treated with caution.

A difference in the elevation of the unconformity between the Renney Slip and Marloes Sands sections has been previously suggested by Hillier (2002), who argued for the presence of an incised lowstand valley fill, situated at Renney Slip, and the onlap of sediment onto the elevated margin of an incised valley at Marloes Sands. Such a difference in elevation can help explain the anomalous changes in the thickness of strata occupied by Fauna II of Walmsley and Bassett (1976), which occurs in the lower part of the Coralliferous Formation. Notably, Fauna II occupies a greater thickness of strata at Renney Slip (Fig. 2), and depending upon the scaling of figure 9 of Walmsley and Bassett (1976) suggests a

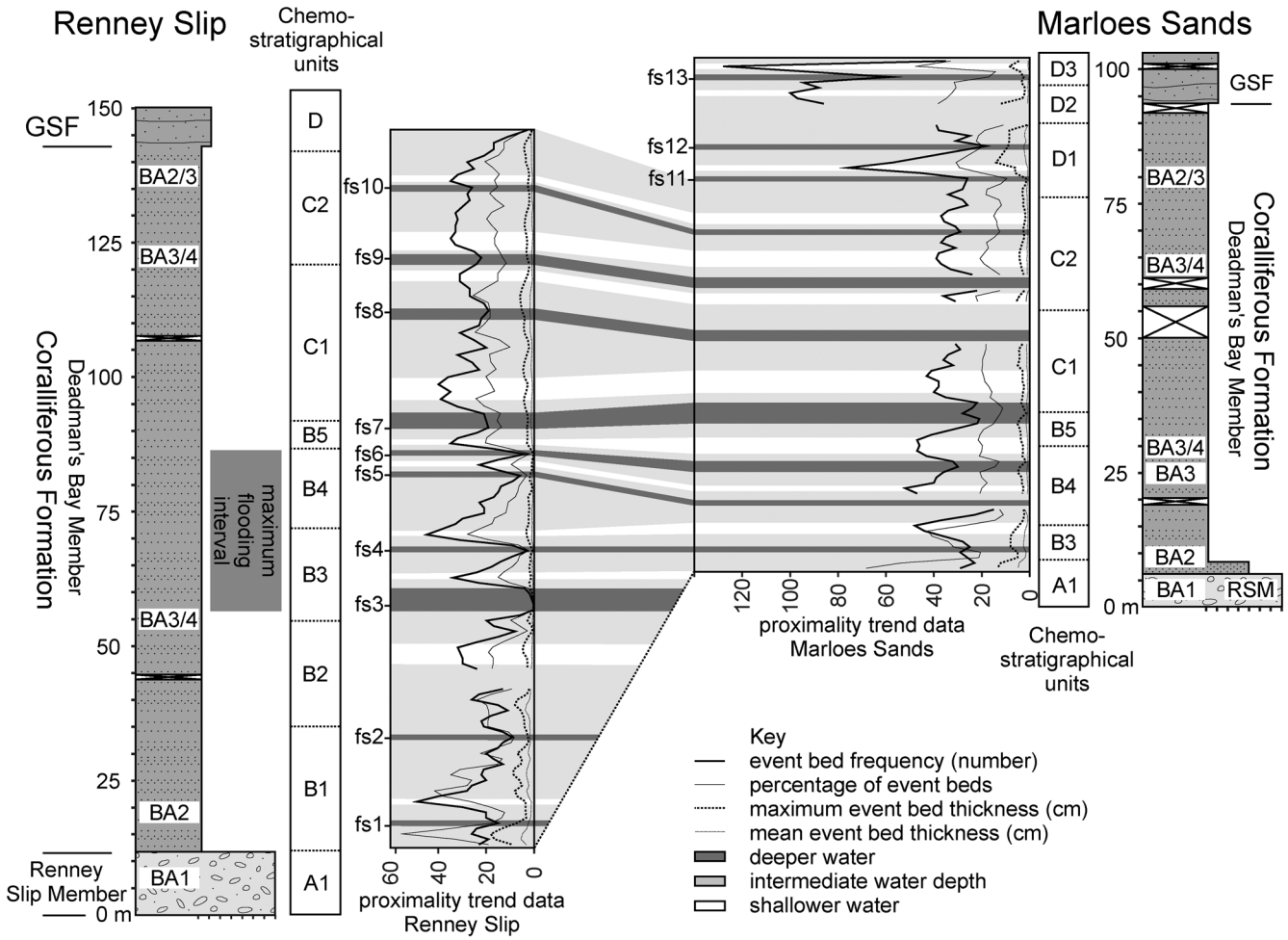

Fig. 5. Proximality trend data for the Deadman's Bay Member in the Renney Slip (left) and Marloes Sands sections (right). The data are plotted using a 3 m sample interval with a three-point moving average to remove small-scale variations. Data plotted are: event bed frequency (number) (bold continuous line; typically largest values); percentage of event beds (fine continuous line; typically second largest values); maximum event bed thickness (cm) (bold dotted line; typically second smallest values); mean event bed thickness (cm) (fine dotted line; typically smallest values). The thickness of discontinuous beds, and those of variable thickness, was taken as their average; bentonites were not counted as event beds. Our interpretation of the sea-level changes responsible for these variations is represented by dark grey (deeper water), white (shallower water) and light grey (intermediate depth). Short-term deepwater maxima have been labelled as flooding surfaces (fs1 to fs13), whereas the medium-term maxima correspond to the maximum flooding interval. Benthic assemblage (BA) zones are given to provide an indication of medium-term sea-level change (see Fig. 2). It should be noted that benthic assemblage zones represent approximate stratigraphic positions derived from the collation of information from multiple sources, which sometimes conflict in detail. Sources: benthic assemblage zones from Walmsley and Bassett (1976) and Aldridge *et al.* (2002).

thinning of *c.* 40–60 m by Marloes Sands, and presumably the onlap of an unconformity of a similar magnitude. More broadly, the 57 m difference in the elevation of the unconformity between Renney Slip and Marloes Sands can be used as an indication of the magnitude of the sea-level rise needed to initiate deposition of the Renney Slip Member across the study area. However, the sedimentology, proximality trends and benthic assemblage zones (see below) show that sea-level continued to rise into the Coralliferous Formation at Marloes Sands, and indicate that the 57 m rise in sea-level is only part of the overall magnitude of transgression.

Changes in water depth in the Coralliferous Formation based upon benthic assemblage zones

Sedimentological interpretation and proximality trends suggest that sea-level continued to rise into the Coralliferous Formation, and this is reflected too in the associated faunas. Walmsley and Bassett (1976) and Aldridge *et al.* (2002) discussed the brachiopod-dominated faunas of the Coralliferous Formation in terms of the benthic assemblages (BA) of Boucot (1975). It was found that many collections did not fall neatly into a single benthic assemblage, perhaps reflecting the originally intergradational nature of assemblages, the effects of local sea-floor topographical variations and transport, or cyclic short-term changes in sea-level. Broadly, Faunas II and III of Walmsley and Bassett (1976), which characterize the bulk of the Coralliferous Formation (Fig. 2), were considered referable to BA3 and possibly BA4 (BA3/4), whereas the overlying Fauna IV was considered closer inshore and probably shallower (BA2/3), reflecting a shallowing trend that continued into the overlying Gray Sandstone Formation (BA2 to BA1). The scarcity of body fossils in the Renney Slip Member has previously precluded the assignment of a benthic assemblage, but the presence of lingulid fragments in a shoreface setting directly above a subaerially exposed unconformity surface (Veevers *et al.* 2007) is suggestive of BA1. Within the overlying Deadman's Bay Member, Aldridge *et al.* (2002) identified BA2 as being associated with an assemblage rich in the brachiopod *Eocoelia sulcata* and the solitary rugose coral *Palaeocyclus porpita*, and BA3 as an assemblage rich in the brachiopod *Costistricklandia lirata lirata* (but lacking *Eocoelia*) plus diverse corals, including favositids and *P. porpita* (Fig. 2). The transition from BA1 to BA3 appears restricted to the lower *c.* 25 m of the Coralliferous Formation in the Marloes Sands section, above which most of the Deadman's Bay Member is considered to represent a more offshore setting (BA3/4). In

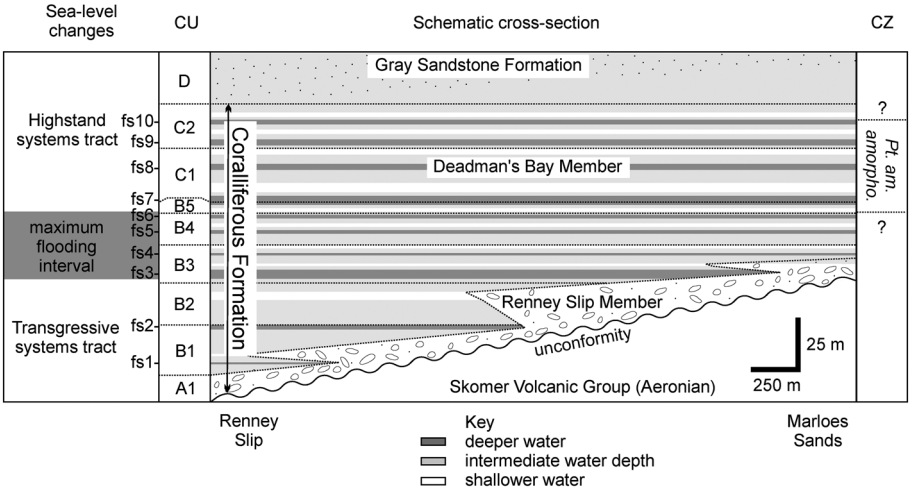

Fig. 6. Schematic cross-section and depositional model of the Coralliferous Formation between Renney Slip and Marloes Sands, a current distance of approximately 3 km. Correlation has been achieved using medium-term (sequence stratigraphic systems tracts and flooding interval) and short-term sea-level changes (e.g. correlation using flooding surfaces (fs4 to fs10)), established from sedimentology, palaeoenvironment and proximality data, alongside chemostratigraphic units (CU). The stratigraphic position of the *Pterospathodus amorphognathoides amorphognathoides* (*Pt. am. amorpho.*) conodont zone (CZ), identified in the Marloes Sand section, is also shown. It should be noted that the correlation and synchronicity of flooding surfaces within chemostratigraphic package D and the base of the Gray Sandstone Formation is unclear owing to an inability to distinguish chemostratigraphic units D1, D2 and D3 at Renney Slip.

sequence stratigraphic terms the benthic assemblages complement the interpretations derived from sedimentology and proximality trends: the succession begins as a transgressive systems tract, culminating in a maximum flooding interval established within the lower part of the Coralliferous Formation, above which stillstand and gentle shallowing occupy the remainder of the formation and indicate a highstand systems tract (Figs 2, 5 and 6).

The precise determination of the absolute water depths associated with benthic assemblages is not possible, but Brett *et al.* (1993) proposed a range of 0–60 m for BA1 to BA4, with BA3 typically represented by an average depth of 30–40 m and BA4 50–60 m; the boundary between BA3 and BA4 is taken at 45 m. Johnson (1987) suggested 0–10 m for BA1 and 10–30 m for BA2. Similarly, proximality trends place the succession in the mid-shelf of Brenchley and Harper (1998), which they suggested to be 20–60 m deep, equivalent to the likely depth range represented by the Deadman's Bay Member. Notably, the BA4–5 boundary, which is not recorded from the succession, is often coincident with the lower end of storm wave base and the photic zone, and its absence indicates that water depths were unlikely to have significantly exceeded 60 m (Johnson 1987; Brett *et al.* 1993). Taking these depth estimates into account, the transgression that deposited the Coralliferous Formation at Marloes Sands was of sufficient magnitude not only to transgress the relief of the unconformity surface (57 m), but also to create the 30–60 m of water depth needed for the development of BA3/4, approximately 25 m into the succession. Furthermore, if it is assumed that the short-term sea-level cycles identified by proximality trend data broadly reflect changes in water depth constrained by their accompanying benthic assemblage, it seems likely that such cycles reflect water depth changes of the order of 10–20 m from the longer-term trend (i.e. benthic assemblages have a typical water depth range of 10–20 m, with 20 m reflecting the difference between upper and lower average estimates of BA3 and BA4).

The magnitude of eustatic sea-level rise within the Coralliferous Formation

Based on distinctive troughs within the proximality data, a medium-term sea-level high (maximum flooding interval) is inferred within chemostratigraphical units B3 to B4, corresponding to an interval within BA3/4 at Renney Slip and the transition from BA2 to BA3/4 at Marloes Sands (Fig. 5). The Marloes Sands section provides the most straightforward assessment of the overall amount of transgression, as it is situated on the more elevated part of the unconformity surface and has the best documented transition from BA1 to BA3, with BA3/4 presumably occurring immediately above and in association with the uppermost short-term flooding surface within the maximum flooding interval. Accordingly, estimates of the total amount of relative sea-level change (i.e. the difference between eustatic sea-level and tectonic subsidence as measured from the top of the pre-Telychian basement) created at Marloes Sands can be estimated where short-term flooding surfaces, within the maximum flooding interval, correspond to a benthic assemblage zone boundary. Notably, the first short-term flooding surface (fs4) that is traceable between Renney Slip and Marloes Sands coincides with BA2 at 10 m above the unconformity, whereas the last of the short-term flooding surfaces (fs6) within the maximum flooding interval occurs at 25 m above the unconformity and in association with BA3/4. By tallying the relief on the unconformity surface (57 m), with the water depth attributed to BA2 (10–30 m) and BA3/4 (30–60 m), and the amount of sediment accumulated by BA2 and BA3/4 (10 and 25 m, respectively), an assessment of the amount of relative sea-level rise may be estimated. Accordingly, this may have reached between 77–97 m by BA2 and 112–142 m by BA3/4. A similar relative sea-level estimate (116–146 m) may be achieved by combining the thickness of sediment accumulated by the top of the maximum flooding interval at Renney Slip (86 m), with the water depth attributed to BA3/4.

If these increases in relative sea-level equated directly to the magnitude of a global transgression, they would be significantly larger than most estimates of Silurian eustasy, and the 60–95 m estimates for the basal Silurian transgression (Brenchley *et al.* 2006; Johnson 2006; Le Heron and Dowdeswell 2009), which resulted from the collapse of the end-Ordovician icecap (Highstand 1 of Johnson 2006). However, subsidence is likely to have contributed significantly to relative sea-level change in the Marloes Sands section, and sedimentation rates were sufficient to moderate the creation of accommodation space, such that water depths never exceeded BA3/4. In particular, a phase of late Llandovery and Wenlock extension, linked to the final stages of the closure of the Iapetus Ocean, affected the Welsh Basin and to a lesser extent the

Midland Platform during the time that the Coralliferous Formation was deposited (Woodcock *et al.* 1996; Cherns *et al.* 2006). A comparison of backstripped, water-loaded subsidence curves for the Midland Platform and Welsh Basin (including a curve for Marloes Sands) indicates that the Marloes area has a similar late Llandovery and Wenlock subsidence history to the Dudley and Wenlock Edge areas, and indicates a tectonic subsidence rate of the order of 40 m Ma^{-1} (Aldridge *et al.* 2000, fig. 1.5). Such an estimate must be treated with caution, owing to significant uncertainties in both the timescale used (Tucker and McKerrow 1995; Aldridge *et al.* 2000, fig. 1.2) and the water depth in which each sedimentary unit was deposited (King 1994; Woodcock *et al.* 1996; Butler *et al.* 1997). Nonetheless a tectonic subsidence rate of 40 m Ma^{-1} is typical of a relatively stable cratonic area (Allen and Allen 2005, pp. 364–366; Xie and Heller 2009), and therefore fits our expectations of the Midland Platform.

To refine further the impact of subsidence on the medium-term transgression identified within the Coralliferous Formation, an understanding of the duration of the transgression is required. Unfortunately, this is significantly constrained by the biostratigraphic limitations of the succession, with the potentially incomplete range of the conodont *Pt. am. amorphognathoides* (Figs 2 and 6) providing the only overlap with the maximum flooding interval and robust link to the international timescale. Above, the Llandovery–Wenlock boundary probably coincides with sea-level fall towards the Coralliferous–Gray Sandstone Formation boundary. Because of this limited age control, it is unclear whether the transgression occurred during much of the duration of the *Pt. am. amorphognathoides* conodont zone (2.6 Myr according to Melchin *et al.* 2020) or was significantly longer or shorter than that zone.

In the absence of more precise biostratigraphic dating, an alternative means of establishing the age of the succession is to attempt to identify the position of the Coralliferous Formation transgression within sea-level curves that depict eustasy (for discussion see Coe and Ray 2022); that is, is there a significant eustatic transgression in association with the *Pt. am. amorphognathoides* conodont zone and below the Llandovery–Wenlock boundary? For the Silurian there are three commonly cited sea-level curves that attempt to depict eustasy (Loydell 1998; Johnson 2006; Haq and Schutter 2008), all of which associate the *Pt. am. amorphognathoides* conodont zone with a phase of transgression, above which sea-level falls near the Llandovery–Wenlock boundary. Both Loydell (1998) and Johnson (2006) provided detailed commentaries on how their curves were constructed and age-calibrated, whereas the Haq and Schutter (2008) curve, which also covers the rest of the Paleozoic, has no such commentary, lacks calibration to biozonal level and is therefore unsuitable for our needs. The curve of Johnson (2006) is based predominantly on shelf successions, which, like the Coralliferous Formation, are difficult to precisely date and are frequently associated with unconformities. This contrasts with the sea-level curve of Loydell (1998), which is based on basinal successions where the precise dating of graptolitic strata is often possible, stratigraphic gaps are reduced and a more detailed sea-level curve can be established.

Using the high-resolution sea-level curve of Loydell (1998) the Coralliferous Formation transgression appears equivalent to a late Telychian sea-level rise, which begins in the *crenulata* graptolite zone and peaked, in association with four minor sea-level cycles and two sea-level maxima, within the *spiralis* to the basal quarter of the *lapworthi* graptolite zones (Fig. 7). The peak of sea-level in the curve of Loydell (1998) is associated with the widespread deposition of graptolitic muds within shelf sequences, with the minor sea-level cycles reflective of bands of high graptolite diversity and the sea-level maxima peaks in shelfal graptolite diversity. As with the Coralliferous Formation maximum flooding interval, there is a partial overlap with the *Pt. am. amorphognathoides* conodont zone in the curve of Loydell (1998), as the base of the *lapworthi* graptolite zone is considered synchronous with the base of the *Pt. am. amorphognathoides* conodont zone (Melchin

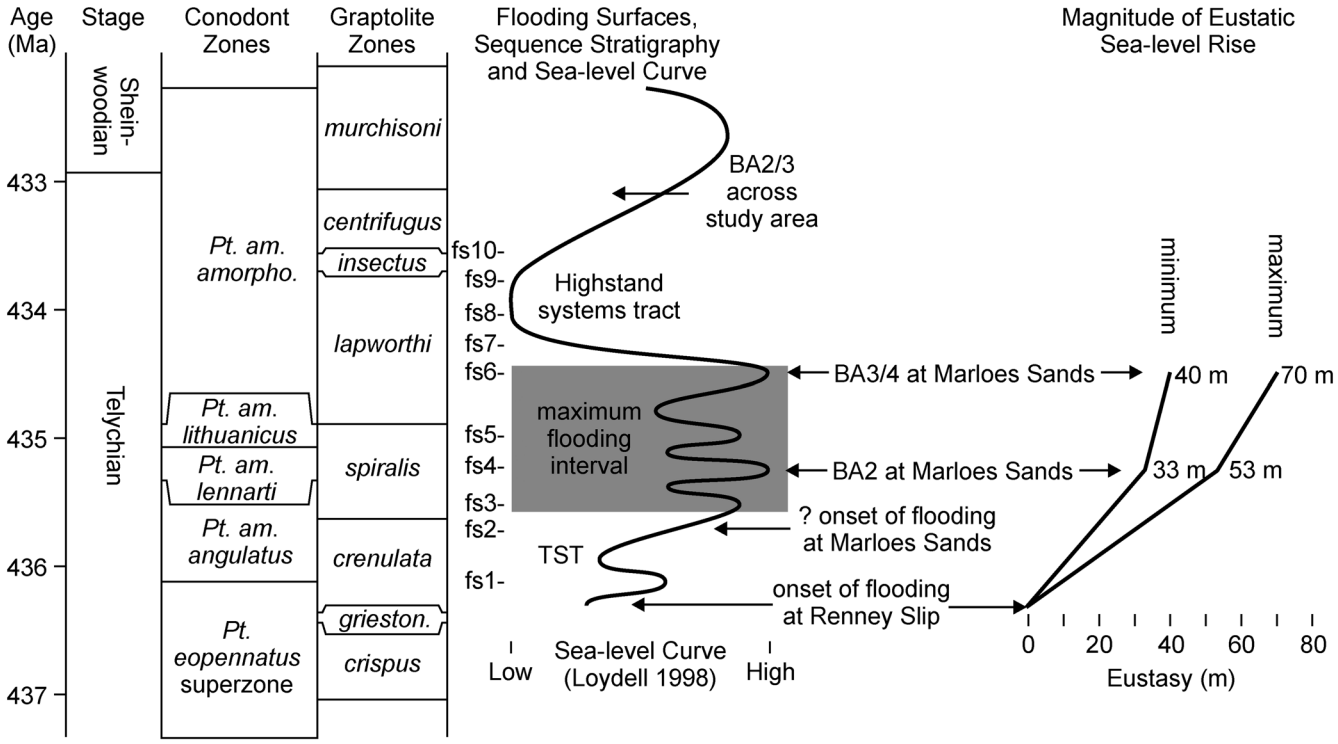

Fig. 7. The sea-level curve of Loydell (1998) calibrated to the Geologic Time Scale 2020, compared with the flooding surfaces (fs1 to fs10) and sequence stratigraphy (TST, transgressive systems tract) derived from the Coralliferous Formation. Minimum and maximum estimates of sea-level rise (m) are given for the eustatic component of the late Telychian transgression at Marloes Sands. Conodont and graptolite zone abbreviations: *Pt.*, *Pterospathodus*; *am.*, *amorphognathoides*; *grieston.*, *griestoniensis*. Source: sea-level curve from Loydell (1998).

et al. 2020). Similarly, the base of the C_6 time interval corresponds to the base of the *crenulata* graptolite biozone and the onset of transgression. Accordingly, the globally expressed late Telychian sea-level rise and accompanying minor sea-level cycles appear to mirror the transgressive systems tract, maximum flooding interval and four short-term sea-level cycles (flooding surfaces) observed within the Coralliferous Formation (Figs 6 and 7). Above the maximum flooding interval, Loydell (1998) identified a major sea-level fall. This regression presumably occurs within the aggradational and progradational deposits of the highstand systems tract in the upper half of the Coralliferous Formation (Figs 6 and 7) but is not an obvious event, probably owing to the counteracting effect of subsidence.

Using the software TimeScale Creator (Lugowski *et al.* 2024) the absolute age of the inflection points on the curve of Loydell (1998) can be calibrated to the Geologic Time Scale 2020, and the duration of the transgression calculated to the two highest points of sea-level within the maximum flooding interval. The onset of the transgression corresponds to the base of the *crenulata* graptolite zone (436.4 Ma), with the first sea-level maximum occurring near the base of the *spiralis* graptolite zone (435.3 Ma) and the second a quarter of the way through the *lapworthi* graptolite zone (434.6 Ma). Based upon these absolute age estimates, the main phase of transgression to the first sea-level maximum occurred over 1.1 Myr, with the second sea-level maximum and end of the maximum flooding interval occurring after a further 0.7 Myr (i.e. 1.8 Myr from the onset of the transgression). Consequently, with an estimated subsidence rate of 40 m Ma^{-1}, the Marloes Sands section could have subsided by 44 m by the first sea-level maximum, and 72 m by the second. By removing tectonic subsidence from values calculated for relative sea-level, a closer approximation to the eustatic contribution to sea-level rise may be determined, with the relative sea-level values achieved by BA2 (77–97 m) revised to 33–53 m of eustatic rise corresponding to the first sea-level maximum, and 40–70 m by the second (was 112–142 m by BA3/4).

Global significance of the Coralliferous Formation sea-level record

The identification of eustatic sea-level changes within the Coralliferous Formation highlights the importance of this succession as an example of Telychian global change. However, the recognition of a medium-term late Telychian sea-level rise within the Coralliferous Formation is perhaps not surprising, in that it is considered the most widely recognized of the Silurian sea-level events, with records in North America, northern Europe, southern Europe, south China and part of Australia (Johnson 2006), and may correspond to the highest point of Silurian sea-level (Loydell 1998). Furthermore, the recognition of traceable short-term sea-level cycles in association with a medium-term sea-level rise highlights the potential utility of combining different orders of sea-level change as a means of further refining correlations. However, the short-term sea-level cycles identified by Loydell (1998) are based upon geographically restricted successions in Eastern Avalonia and Baltica, with the three short-term sea-level cycles of the *spiralis* graptolite zone seemingly based upon three high-diversity graptolitic levels in the succession at Buttington Brick Pit, Powys, Wales (Loydell 1998); the other cited sections show a range in the number of graptolitic levels from a single level at Kilbride Peninsula, County Mayo, Ireland, to four levels in the Banwy River section, Wales, and to at least 20 graptolitic levels within the Ohesaare core, Estonia. Nonetheless the graptolitic levels at Buttington Brick Pit do provide age constraints for the sea-level rise, and the middle level that belongs to the middle of the *spiralis* graptolite zone contains the most diverse graptolite fauna (Loydell and Cave 1993), thereby indicating the most distal setting. This is commonly the case for the middle *spiralis* graptolite zone (e.g. in the Ohesaare core, Estonia and Kilbride Peninsula, Ireland). Accordingly, although the exact number of globally expressed short-term sea-level cycles is unclear, the maxima of the late Telychian sea-level rise are well represented by the curve of Loydell (1998), and the Coralliferous Formation provides further support for the identification of four short-term cycles attributed to that maximum flooding interval.

Although there are significant uncertainties in our approach for establishing the magnitude of late Telychian sea-level rise (e.g. in estimating the water depth, subsidence history and the duration of transgression) the resulting estimate of eustatic sea-level rise is in line with other estimates. Notably, Highstand 4 of Johnson (2006), which appears age equivalent to the Coralliferous Formation transgression, is associated with the transgression of an unconformity with a topographic relief of 50 m on Anticosti Island, Canada (Desrochers 2006; Johnson 2006), and a karstic relief of 53 m in Illinois and Wisconsin, USA (Johnson *et al.* 1998). Notably, these examples estimate sea-level rise based upon measurements of the relief and onlap of an unconformity surface, and as such are directly comparable with the relief of the unconformity surface between Renney Slip and Marloes (57 m). However, these examples do not include the water depths attributed to sediments that onlap and bury their unconformities and do not take account of subsidence, and as such are estimates of the minimum amount of relative sea-level rise, rather than eustasy. Nonetheless, they act as useful approximations for the magnitude of Telychian eustatic change, have a similar relief to the unconformity in this study (57 m) and indicate that our peak in eustatic sea-level rise of between 40 and 70 m, with a mean of 55 m, seems plausible for the globally expressed late Telychian sea-level rise.

The precise duration of the medium- and short-term sea-level cycles observed within the Coralliferous Formation is difficult to establish with confidence, owing primarily to limited Telychian absolute age constraint within the Geologic Time Scale 2020 (Melchin *et al.* 2020) and the correlation of the Coralliferous Formation with that timescale. Accordingly, identifying the specific orbital forcing cycles believed to control medium- to short-term eustasy (Simmons *et al.* 2020) within the Coralliferous Formation is necessarily speculative. Nonetheless, our age assessment indicates that cycles range from a few millions of years (based upon a 1.8 Myr late Telychian sea-level rise) to a few hundreds of thousands of years (0.3 Myr based upon six short-term cycles during the late Telychian sea-level rise (Figs 5 and 7)). Although these durations do not directly accord with the eccentricity or long-period obliquity cycles of orbital forcing (0.1, 0.4, 2.4 and 1.2 Myr, respectively), they are of a duration indicative of the climate-linked drivers of eustasy (i.e. glacio-, thermo- and aquifer- eustasy) (Simmons *et al.* 2020, fig. 13.6).

Eustatic changes greater than a few tens of metres are indicative of glacio-eustasy, even during the warmest of geological times (Davies *et al.* 2020, fig. 7). An obvious prerequisite for glacio-eustasy in the Silurian is the presence of waxing and waning ice sheets, and evidence of terrestrial ice sheets within the Silurian is well established, with glacial deposits reported from areas of Gondwana, notably South America, situated near the palaeo-South Pole (Grahn and Caputo 1992; Caputo 1998; Díaz-Martínez and Grahn 2007; Cuervo *et al.* 2018). In addition, $\delta^{18}O$ records indicate a highly dynamic Silurian climate with cooling events (positive $\delta^{18}O$ maxima) rivalling those during the preceding, and well-established, Hirnantian (end-Ordovician) ice-age (Trotter *et al.* 2016; Goldman *et al.* 2020). Accordingly, glacio-eustasy seems the most plausible mechanism for driving global sea-level change within the Silurian generally and more specifically the Telychian of the Coralliferous Formation.

Given the probable glacio-eustatic origin of sea-level cycles within the Coralliferous Formation, their magnitude can be used as a means of comparison with glacial episodes within the underlying

Silurian and Ordovician, and as a proxy for the volume of ice sheets. Based on a comparison of magnitude estimates (Johnson 2006) there is a progressive decline in the magnitude of sea-level changes throughout the Llandovery (i.e. Rhuddanian 70 m, Aeronian 63 m, Telychian 50 and 53 m), which is suggestive of a decrease in the size of Llandovery ice sheets, from a maximum within the earlier Hirnantian ice-age. This inferred reduction in ice sheet size is accompanied by a broad warming trend, as identified from $\delta^{18}O$ records, which peak within the Telychian (Trotter *et al.* 2016; Melchin *et al.* 2020). In detail, oxygen isotope data from Estonia indicate that the Telychian climate was variable, with short-term positive and negative shifts in $\delta^{18}O$ suggesting changes in sea surface temperature of the order of 2–5°C (Lehnert *et al.* 2010). Prior to the Hirnantian ice-age, Katian sea-level cycles from the Bou Ingarf succession in Morocco indicate similar durations and magnitudes to those in the Coralliferous Formation, and have been attributed to glacio-eustasy (Loi *et al.* 2010; Simmons *et al.* 2020). Notably, medium-term cycles (1.4–2.7 Myr) have magnitudes of the order of 30–50 m, whereas short-term magnitudes are of the order of 10–30 m and have been linked to 0.4 Myr eccentricity cycles. These interpretations of glacio-eustasy within the Katian and Llandovery support the notion of persistent pre- and post-Hirnantian ice sheets: the Early Paleozoic Icehouse of Page *et al.* (2007). As regards the size of the ice sheet needed to melt to generate the late Telychian sea-level rise, this can be based upon a simple ice volume to sea-level rise calculation (Le Heron and Dowdeswell 2009), with the mean estimate of late Telychian sea-level rise (55 m) requiring the melting of 20.1×10^6 km^3 of land-grounded ice, a volume that is approximately equivalent to the present-day East Antarctica ice sheet (Lythe and Vaughan 2001). Accordingly, substantial ice sheets must have existed within the Telychian, and although the deglaciation associated with the late Telychian sea-level rise would have reduced their aggregate size significantly, this was only temporary, as the overlying Sheinwoodian is marked by pronounced climate cooling, sea-level changes and associated glacial deposits, the Sheinwoodian Glaciation (Johnson 2006; Lehnert *et al.* 2010; Trotter *et al.* 2016).

Conclusions

(1) Detailed subdivision and internal correlation of the Coralliferous Formation has been achieved by utilizing variations in the geochemical characteristics of 47 major, trace and rare earth elements. Chemical logs for selected key ratios have been used to identify four statistically robust geochemical packages, which have been further subdivided into 11 units. Some chemostratigraphical units can be traced between the Renney Slip and Marloes Sands sections, whereas others are locally absent. The presence of additional units at Renney Slip is reflected in a thickening (+50.26 m) of Package B there, and suggests a significant local hiatus at Marloes Sands.

(2) The Renney Slip Member is interpreted as a transgressive deposit linked to the initial flooding of the area, and is likely to be time-transgressive, as is its chemostratigraphical signature (Package A).

(3) The alternating lithologies that dominate the Deadman's Bay Member represent deposition during quiet 'background' conditions (the silty mudstones) and higher energy, periodic events (the sandstones, shelly sandstones and bioclastic beds); variations in these lithologies are of use for establishing proximality trends and identifying potentially traceable sea-level cycles.

(4) Troughs in the proximality data, where values approach or reach zero, reflect deepening maxima near the lower limits of storm sedimentation. These are evident only in chemostratigraphical units B3 and B4 at Renney Slip, thereby identifying this as the most distal part of the succession and representing the stratigraphic position of a medium-term sea-level high (maximum flooding interval). This is consistent with Renney Slip being the first section to be transgressed by the sea and accounts for the absence of chemostratigraphical units B1 to lower B3 at Marloes Sands.

(5) The Coralliferous Formation between the Renney Slip and Marloes Sands sections was deposited over an unconformity surface eroded into an elevated area of basement. Differences in the palaeo-relief of the unconformity surface can be estimated by variations in the thickness of the onlapping Coralliferous Formation, and indicate a 57 m difference in elevation between Renney Slip and Marloes Sands.

(6) Changes in benthic assemblage zones reflect a medium-term transgressive–regressive cycle of sea-level change within the Coralliferous Formation. The transgression begins with a shift from BA1 to BA3 within the lower *c.* 25 m of the Coralliferous Formation, above which BA3/4 represents the most offshore setting and a probable water depth of between 30 and 60 m. Near the top of the formation BA2/3 indicates a shallowing into the Gray Sandstone Formation.

(7) The maximum flooding interval at Marloes Sands was reached by the transgression of the unconformity relief (57 m) and an increase in water depth to BA3/4 (30–60 m) by 25 m stratigraphically into the onlapping succession. This suggests an increase in relative sea-level between 112 and 142 m, although subsidence is likely to have significantly contributed to relative sea-level rise.

(8) Comparisons with the eustatic sea-level curve of Loydell (1998) suggest that the Coralliferous Formation transgression is equivalent to a late Telychian sea-level rise. Based upon absolute age estimates from the Geologic Time Scale 2020 and subsidence rates for the Marloes area (40 m Ma^{-1}) the calculated eustatic rise in sea-level is likely to be of the order of 40–70 m, with a mean of 55 m.

(9) The eustatic origin, duration and magnitude of the sea-level cycles within the Coralliferous Formation are indicative of orbitally driven glacio-eustasy. Notably, a glacio-eustatic sea-level rise of 55 m requires the melting of 20.1×10^6 km^3 of land-grounded ice, a volume that is approximately equivalent to the present-day East Antarctica ice sheet. These interpretations support the notion that the waxing and waning of persistent post-Hirnantian ice sheets was an important driver of Silurian sea-level change.

Scientific editing by Xiaoya Ma

Acknowledgements The authors would like to thank Chemostrat for supplying inorganic geochemical data. The paper benefitted from constructive reviews by R. D. Hillier and an anonymous reviewer, as well as from comments on an earlier version of the paper by D. A. T. Harper and M. P. Smith. P. Männik is acknowledged for his helpful insights into conodont collections from Marloes Sands, and D. K. Loydell is thanked for discussions upon the construction of his sea-level curve. The expert seamanship of B. Dilley facilitated access to Deadman's Bay to collect samples.

Author contributions **SJV**: conceptualization (lead), data curation (lead), formal analysis (lead), funding acquisition (supporting), investigation (lead), methodology (lead), project administration (lead), resources (supporting), software (lead), visualization (supporting), writing – original draft (lead), writing – review & editing (supporting); **DCR**: methodology (supporting), visualization (supporting), writing – review & editing (lead); **KTR**: methodology (supporting), resources (supporting), software (supporting), supervision (supporting), validation (supporting), visualization (supporting), writing – original draft (supporting), writing – review & editing (supporting); **ATT**: conceptualization (lead), formal analysis (supporting), funding acquisition (lead), investigation (supporting), methodology (supporting), project administration (supporting), resources

(lead), software (supporting), supervision (lead), validation (lead), visualization (supporting), writing – original draft (supporting), writing – review & editing (supporting).

Funding S.J.V. acknowledges a University of Birmingham School Studentship and additional fieldwork funding from W. S. Atkins (Birmingham).

Competing interests The authors declare that they have no known competing financial interests or personal relationships that could have appeared to influence the work reported in this paper.

Data availability The datasets generated during the current study are available in the PhD thesis of Veevers (2006).

References

Aigner, T. (ed.) 1985. *Storm Depositional Systems: Dynamic Stratigraphy in Modern and Ancient Shallow-Marine Sequences*. Lecture Notes in Earth Sciences, **3**, https://doi.org/10.1007/BFb0011413

Aigner, T. and Reineck, H.E. 1982. Proximality trends in modern storm sands from the Heligoland Bight (North Sea) and their implications for basin analysis. *Senckenbergiana Maritima*, **14**, 183–215.

Aldridge, R.J., Siveter, D., Siveter, D., Lane, P.D., Palmer, D.G. and Woodcock, N.H. 2000. *British Silurian Stratigraphy*. Geological Conservation Review Series, **19**.

Aldridge, R.J., Bassett, M.G. *et al.*. 2002. Telychian rocks in the British Isles. *National Museum of Wales, Geological Series*, **21**, 43–72.

Allen, P.A. and Allen, J.R. 2005. *Basin Analysis: Principles and Applications*, 2nd edn. Wiley-Blackwell.

Allen, J.R.L. and Williams, B.P.J. 1978. The sequence of the earlier lower Old Red Sandstone (Siluro-Devonian), north of Milford Haven, southwest Dyfed (Wales). *Geological Journal*, **13**, 113–136, https://doi.org/10.1002/gj.3350130202

Baarli, B.G. 1988. Bathymetric co-ordination of proximality trends and level-bottom communities: a case study from the Lower Silurian of Norway. *Palaios*, **3**, 577–587, https://doi.org/10.2307/3514446

Baarli, B.G. 1998. Silurian cycles and proximality-trend analysis of tempestite deposits. *In*: Landing, E. and Johnson, M.E. (eds) *Silurian Cycles: Linkages of Dynamic Stratigraphy with Atmospheric, Oceanic, and Tectonic Changes*. New York State Museum, 75–88.

Bassett, M.G. and Rong, J.-Y. 2002. Brachiopods. *National Museum of Wales, Geological Series*, **21**, 124–136.

Boucot, A.J. 1975. *Evolution and Extinction Rate Controls*. *Developments in Palaeontology and Stratigraphy*, **1**.

Brenchley, P.J. and Harper, D.A.T. 1998. *Palaeoecology: Ecosystems, Environments and Evolution*. Routledge.

Brenchley, P.J., Marshall, J.D., Harper, D.A.T., Buttler, C.J. and Underwood, C.J. 2006. A Late Ordovician (Hirnantian) karstic surface in a submarine channel, recording glacio-eustatic sea-level changes: Meifod, central Wales. *Geological Journal*, **41**, 1–22, https://doi.org/10.1002/gj.1029

Brett, C.E., Boucot, A.J. and Jones, B. 1993. Absolute depths of Silurian benthic assemblages. *Lethaia*, **26**, 25–40, https://doi.org/10.1111/j.1502-3931.1993.tb01507.x

Butler, A.J., Woodcock, N.H. and Stewart, D.M. 1997. The Woolhope and Usk Basins: Silurian rift basins revealed by subsurface mapping of the southern Welsh Borderland. *Journal of the Geological Society, London*, **154**, 209–223, https://doi.org/10.1144/gsjgs.154.2.0209

Caputo, M.V. 1998. Ordovician–Silurian glaciations and global sea-level changes. *In*: Landing, E. and Johnson, M.E. (eds) *Silurian Cycles: Linkages of Dynamic Stratigraphy with Atmospheric, Oceanic, and Tectonic Changes*. New York State Museum, 15–25.

Cherns, L., Cocks, L.R.M., Davies, J.R., Hillier, R.D., Waters, R.A. and Williams, M. 2006. Silurian: the influence of extensional tectonics and sea-level changes on sedimentation in the Welsh Basin and on the Midland Platform. *In*: Brenchley, P.J. and Rawson, P.F. (eds) *The Geology of England and Wales*. Geological Society, London, 75–102, http://dx.doi.org/10.1144/GOEWP.4

Clayton, C.J. 1994. A rock volume accumulation curve for the Late Ordovician–Silurian Welsh Basin. *Geological Magazine*, **131**, 539–544, https://doi.org/10.1017/S0016756800012140

Cocks, L.R.M., Holland, C.H. and Richards, R.B. 1992. *Revised Correlation of Silurian Rocks in the British Isles*. Special Report, **21**. Geological Society, London.

Coe, A.L. and Ray, D.C. 2022. Sequence stratigraphy: using changes in relative sea-level and sediment supply to divide, correlate and understand the stratigraphical record. *GSL Geoscience in Practice*, 141–160, https://www.geolsoc.org.uk/GIP001

Cotter, E. 1988. Hierarchy of sea-level cycles in the medial Silurian siliciclastic succession of Pennsylvania. *Geology*, **16**, 242–245, https://doi.org/10.1130/0091-7613(1988)016<0242:HOSLCI>2.3.CO;2

Craigie, N. 2018. *Principles of Elemental Chemostratigraphy*. Advances in Oil and Gas Exploration & Production, https://doi.org/10.1007/978-3-319-71216-1

Cramer, B.D., Brett, C.E. *et al.* 2011. Revised correlation of Silurian Provincial Series of North America with global and regional chronostratigraphic units and $\delta^{13}C_{carb}$ chemostratigraphy. *Lethaia*, **44**, 185–202, https://doi.org/10.1111/j.1502-3931.2010.00234.x

Cuervo, H.D.R., Soares, E.A.A., Caputo, M.V. and Dino, R. 2018. Sedimentology and stratigraphy of new outcrops of Silurian glaciomarine strata in the Presidente Figueiredo region, northwestern margin of the Amazonas Basin. *Journal of South American Earth Sciences*, **85**, 43–56, https://doi.org/10.1016/j.jsames.2018.04.023

Dahlqvist, P. 2004. Late Ordovician (Hirnantian) depositional pattern and sea-level change in shallow marine to shoreface cycles in central Sweden. *Geological Magazine*, **141**, 605–616, https://doi.org/10.1017/S0016756804009446

Davies, A., Gréselle, B. *et al.* 2020. Assessing the impact of aquifer-eustasy on short-term Cretaceous sea-level. *Cretaceous Research*, **112**, 104445, https://doi.org/10.1016/j.cretres.2020.104445

De La Beche, H.T. 1846. On the formation of the rocks of South Wales and South Western England. *Memoir of the Geological Survey of the United Kingdom*, **1**, 1–196.

Desrochers, A. 2006. Rocky shoreline deposits in the Lower Silurian (upper Llandovery, Telychian) Chicotte Formation, Anticosti Island, Quebec. *Canadian Journal of Earth Sciences*, **43**, 1205–1214, https://doi.org/10.1139/e06-054

Díaz-Martínez, E. and Grahn, Y. 2007. Early Silurian glaciation along the western margin of Gondwana (Peru, Bolivia and northern Argentina): palaeogeographic and geodynamic setting. *Palaeogeography, Palaeoclimatology, Palaeoecology*, **245**, 62–81, https://doi.org/10.1016/j.palaeo.2006.02.018

Dunne, W.M. 1983. Tectonic evolution of SW Wales during the Upper Palaeozoic. *Journal of the Geological Society, London*, **140**, 257–265, https://doi.org/10.1144/gsjgs.140.2.0257

Easthouse, K.A. and Driese, S.G. 1988. Paleobathymetry of a Silurian Shelf System: application of proximality trends and trace-fossil distributions. *Palaios*, **3**, 473–486, https://doi.org/10.2307/3514721

Goldman, D., Sadler, P.M., Leslie, S.A., Melchin, M.J., Agterberg, F.P. and Gradstein, F.M. 2020. The Ordovician Period. *In*: Gradstein, F.M., Ogg, J.G., Schmitz, M.D. and Ogg, G.M. (eds) *Geologic Time Scale 2020*. Elsevier, 631–694, https://doi.org/10.1016/B978-0-12-824360-2.00020-6

Grahn, Y. and Caputo, M.V. 1992. Early Silurian glaciations in Brazil. *Palaeogeography, Palaeoclimatology, Palaeoecology*, **99**, 9–15, https://doi.org/10.1016/0031-0182(92)90003-N

Haq, B.U. and Schutter, S.R. 2008. A chronology of Paleozoic sea-level changes. *Science*, **322**, 64–68, https://doi.org/10.1126/science.1161648

Hillier, R.D. 2002. Depositional environment and sequence architecture of the Silurian Coralliferous Group, Southern Pembrokeshire, UK. *Geological Journal*, **37**, 247–268, https://doi.org/10.1002/gj.910

Hillier, R.D. and Morrissey, L.B. 2010. Process regime change on a Silurian siliciclastic shelf: controlling influences on deposition of the Gray Sandstone Formation, Pembrokeshire, UK. *Geological Journal*, **45**, 26–58, https://doi.org/10.1002/gj.1165

Huff, W.D. 2016. K-bentonites: a review. *American Mineralogist*, **101**, 43–70, https://doi.org/10.2138/am-2016-5339

Huff, W.D., Morgan, D.J. and Rundle, C.C. 1996. *Silurian K-Bentonites of the Welsh Borderlands: Geochemistry, Mineralogy and K–Ar Ages of Illitization*. British Geological Survey Technical Report, **WG/96/45**.

Hurst, J.M., Hancock, N.J. and McKerrow, W.S. 1978. Wenlock stratigraphy and palaeogeography of Wales and the Welsh Borderland. *Proceedings of the Geologists' Association*, **89**, 197–226, https://doi.org/10.1016/S0016-7878(78)80012-1

Jarvis, I. and Jarvis, K.E. 1992. Plasma spectrometry in the earth sciences: techniques, applications and future trends. *Chemical Geology*, **95**, 1–33, https://doi.org/10.1016/0009-2541(92)90041-3

Johnson, M.E. 1987. Extent and bathymetry of North American Platform Seas in the Early Silurian. *Paleoceanography*, **2**, 185–211, https://doi.org/10.1029/PA002i002p00185

Johnson, M.E. 1992. Studies on Ancient Rocky Shores: a brief history and annotated bibliography. *Journal of Coastal Research*, **8**, 797–812.

Johnson, M.E. 2006. Relationship of Silurian sea-level fluctuations to oceanic episodes and events. *GFF*, **128**, 115–121, https://doi.org/10.1080/11035890601282115

Johnson, M.E. 2023. *Islands in Deep Time: Ancient Landscapes Lost and Found*. Columbia University Press.

Johnson, M.E., Rong, J.-Y. and Kershaw, S. 1998. Calibrating Silurian eustasy against the erosion and burial of coastal paleotopography. *In*: Landing, E. and Johnson, M.E. (eds) *Silurian Cycles: Linkages of Dynamic Stratigraphy with Atmospheric, Oceanic, and Tectonic Changes*. New York State Museum, 3–13.

Kauffman, E.G., Elder, W.P. and Sageman, B.B. 1991. High-resolution correlation: a new tool in chronostratigraphy. *In*: Einsele, G., Ricken, W. and Seilacher, A. (eds) *Cycles and Events in Stratigraphy*. Springer, 795–819.

King, L.M. 1994. Subsidence analysis of Eastern Avalonian sequences: implications for Iapetus closure. *Journal of the Geological Society, London*, **151**, 647–657, https://doi.org/10.1144/gsjgs.151.4.0647

Lamb, M.P., Myrow, P.M., Lukens, C., Houck, K. and Strauss, J. 2008. Deposits from wave-influenced turbidity currents: Pennsylvanian Minturn Formation,

Colorado, U.S.A. *Journal of Sedimentary Research*, **78**, 480–498, https://doi.org/10.2110/jsr.2008.052
Le Heron, D.P. and Dowdeswell, J.A. 2009. Calculating ice volumes and ice flux to constrain the dimensions of a 440 Ma North African ice sheet. *Journal of the Geological Society, London*, **166**, 277–281, https://doi.org/10.1144/0016-76492008-087
Lehnert, O., Männik, P., Joachimski, M.M., Calner, M. and Frýda, J. 2010. Palaeoclimate perturbations before the Sheinwoodian glaciation: a trigger for extinctions during the 'Ireviken Event'. *Palaeogeography, Palaeoclimatology, Palaeoecology*, **296**, 320–331, https://doi.org/10.1016/j.palaeo.2010.01.009
Loi, A., Ghienne, J.-F. *et al.* 2010. The Late Ordovician glacio-eustatic record from a high-latitude storm-dominated shelf succession: the Bou Ingarf section (Anti-Atlas, southern Morocco). *Palaeogeography, Palaeoclimatology, Palaeoecology*, **296**, 332–358, https://doi.org/10.1016/j.palaeo.2010.01.018
Loydell, D.K. 1998. Early Silurian sea-level changes. *Geological Magazine*, **135**, 447–471, https://doi.org/10.1017/S0016756898008917
Loydell, D.K. and Cave, R. 1993. The Telychian (Upper Llandovery) stratigraphy of Buttington Brick Pit, Wales. *Newsletters on Stratigraphy*, **29**, 91–103, https://doi.org/10.1127/nos/29/1993/91
Lugowski, A., Ault, A., Zehady, A.K., Chunduru, N.V., Gangi, P. and Ogg, N. 2024. TSCreator. Geologic TimeScale Foundation, Purdue University.
Lythe, M.B. and Vaughan, D.G. 2001. BEDMAP: a new ice thickness and subglacial topographic model of Antarctica. *Journal of Geophysical Research: Solid Earth*, **106**, 11335–11351, https://doi.org/10.1029/2000JB900449
Mabillard, J.E. and Aldridge, R.J. 1983. Conodonts from the Coralliferous Group (Silurian) of Marloes Bay, south-west Dyfed, Wales. *Geologica et Palaeontologica*, **17**, 29–43.
Männik, P. 2007. An updated Telychian (Late Llandovery, Silurian) conodont zonation based on Baltic faunas. *Lethaia*, **40**, 45–60, https://doi.org/10.1111/j.1502-3931.2006.00005.x
Männik, P. and Aldridge, R.J. 1989. Evolution, taxonomy and relationships of the Silurian conodont, *Pterospathodus*. *Palaeontology*, **32**, 893–906.
Melchin, M.J., Sadler, P.M. and Cramer, B.D. 2020. The Silurian Period. *In*: Gradstein, F.M., Ogg, J.G., Schmitz, M.D. and Ogg, G.M. (eds) *Geologic Time Scale 2020*, **2**. Elsevier, 695–732.
Murchison, R.I. 1839. *The Silurian System, Part 1. Founded on Geological Researches in the Counties of Salop, Hereford, Radnor, Montgomery, Caermarthen, Brecon, Pembroke, Monmouth, Gloucester, Worcester, and Stafford; with Descriptions of the Coal-Fields and Overlying Formations*. 1st edn. John Murray.
Mutti, E., Davoli, G., Tinterri, R. and Zavala, C. 1996. The importance of ancient fluvio-deltaic systems dominated by catastrophic flooding in tectonically active basins. *Memorie di Scienze Geologische, Universita di Padova*, **48**, 233–291.
Myrow, P.M. and Southard, J.B. 1996. Tempestite deposition. *Journal of Sedimentary Research*, **66**, 875–887, https://doi.org/10.1306/D426842D-2B26-11D7-8648000102C1865D
Myrow, P.M., Fischer, W. and Goodge, J.W. 2002. Wave-modified turbidites: combined-flow shoreline and shelf deposits, Cambrian, Antarctica. *Journal of Sedimentary Research*, **72**, 641–656, https://doi.org/10.1306/022102720641
Page, A.A., Zalasiewicz, J.A., Williams, M. and Popov, L.E. 2007. Were transgressive black shales a negative feedback modulating glacioeustasy in the Early Palaeozoic Icehouse? *In*: Williams, M., Haywood, A.M., Gregory, F.J. and Schmidt, D.N. (eds) *Deep Time Perspectives on Climate Change: Marrying the Signal From Computer Models and Biological Proxies*. Geological Society, London, 123–156.
Pearce, T.J., Besly, B.M., Wray, D.S. and Wright, D.K. 1999. Chemostratigraphy: a method to improve interwell correlation in barren sequences – a case study using onshore Duckmantian/Stephanian sequences (West Midlands, U.K.). *Sedimentary Geology*, **124**, 197–220, https://doi.org/10.1016/S0037-0738(98)00128-6
Pearce, T.J., Wray, D.S., Ratcliffe, K.T., Wright, D.K. and Moscariello, A. 2005. Chemostratigraphy of the Upper Carboniferous Schooner Formation, southern North Sea. *In*: Collinson, J.D., Evans, D.J., Holliday, D.W. and Jones, N.S. (eds) *Carboniferous Hydrocarbon Geology in the Southern North Sea and Surrounding Onshore Areas*. Occasional Publication Series, **7**. Yorkshire Geological Society, 47–164.
Pemberton, S.G., Spila, M., Pulham, A.J., Saunders, T., MacEachern, J.A., Robbins, D. and Sinclair, I.K. 2001. *Ichnology and Sedimentology of Shallow to Marginal Marine Systems: Ben Nevis & Avalon Reservoirs, Jeanne d'Arc Basin*. Geological Association of Canada.
Powell, C.M. 1987. Inversion tectonics in S.W. Dyfed. *Proceedings of the Geologists' Association*, **98**, 193–203, https://doi.org/10.1016/S0016-7878(87)80037-8
Powell, C.M. 1989. Structural controls on Palaeozoic basin evolution and inversion in southwest Wales. *Journal of the Geological Society, London*, **146**, 439–446, https://doi.org/10.1144/gsjgs.146.3.0439
Puig López, J.M., Howell, J., Roetzel, R. and Poyatos-Moré, M. 2023. Transgressive rocky coasts in the geological record: insights from Miocene granitic rocky shorelines and modern examples. *Sedimentary Geology*, **446**, 106344, https://doi.org/10.1016/j.sedgeo.2023.106344
Ratcliffe, K.T., Martin, J., Pearce, T.J., Hughes, A.D., Lawton, D.E., Wray, D.S. and Bessa, F. 2006. A regional chemostratigraphically-defined correlation framework for the late Triassic TAG-I Formation in Blocks 402 and 405a, Algeria. *Petroleum Geoscience*, **12**, 3–12, https://doi.org/10.1144/1354-079305-669
Ratcliffe, K., Wright, M., Montgomery, P., Palfrey, A., Vonk, A., Vermeulen, J. and Barrett, M. 2010. Application of chemostratigraphy to the Mungaroo Formation, the Gorgon field, offshore northwest Australia. *Australian Petroleum Production and Exploration Association Journal*, **50**, 371–388, https://doi.org/10.1071/AJ09022
Ratcliffe, K.T., Wright, A.M. and Schmidt, K. 2012. Application of inorganic whole-rock geochemistry to shale resource plays: an example from the Eagle Ford Shale Formation, Texas. *Sedimentary Record*, **10**, 4–9, https://doi.org/10.2110/sedred.2012.2.4
Ratcliffe, K.T., Wilson, A., Payenberg, T., Rittersbacher, A., Hildred, G.V. and Flint, S.S. 2015. Ground truthing chemostratigraphic correlations in fluvial systems. *AAPG Bulletin*, **99**, 155–180, https://doi.org/10.1306/06051413120
Ray, D.C. 2007. The correlation of Lower Wenlock Series (Silurian) bentonites from the Lower Hill Farm and Eastnor Park boreholes, Midland Platform, England. *Proceedings of the Geologists' Association*, **118**, 175–185, https://doi.org/10.1016/S0016-7878(07)80034-4
Ray, D.C., Jarochowska, E., Hughes, H.E. and Wheeley, J.R. 2019. Non-biostratigraphic correlation techniques and their role in stratigraphy: examples from the Wenlock Series (Silurian) of the Midland Platform, England. *Proceedings of the Open University Geological Society*, **5**, 59–64.
Ray, D.C., Jarochowska, E., Röstel, P., Worton, G., Munnecke, A., Wheeley, J.R. and Boomer, I. 2020. High-resolution correlation of the Homerian carbon isotope excursion (Silurian) across the interior of the Midland Platform (Avalonia), UK. *Geological Magazine*, **157**, 603–620, https://doi.org/10.1017/S0016756819001146
Ray, D.C., Gréselle, B. and Nicoll, G. 2021. Non-biostratigraphic techniques in exploration. *In*: Head, R. and Simmons, M.D. (eds) *Exploration Handbook*. Halliburton, 76–83.
Rees, A.J., Thomas, A.T., Lewis, M., Hughes, H.E. and Turner, P. 2014. Lithostratigraphy and palaeoenvironments of the Cambrian in SW Wales. *Geological Society, London, Memoirs*, **42**, 33–100, https://doi.org/10.1144/M42.2
Rickards, R.B. and Chen, X. 2002. Graptolites. *National Museum of Wales, Geological Series*, **21**, 73–83.
Rust, B.R. and Gibling, M.R. 1990. Three-dimensional antidunes as HCS mimics in a fluvial sandstone; the Pennsylvanian South Bar Formation near Sydney, Nova Scotia. *Journal of Sedimentary Research*, **60**, 540–548, https://doi.org/10.2110/60.4.540
Sanzen-Baker, I. 1972. Stratigraphical relationships and sedimentary environments of the Silurian – early Old Red Sandstone of Pembrokeshire. *Proceedings of the Geologists' Association*, **83**, 139–164, https://doi.org/10.1016/S0016-7878(72)80002-6
Scrutton, C.T. and Deng, Z.-Q. 2002. Rugose and tabulate corals. *National Museum of Wales, Geological Series*, **21**, 102–124.
Seilacher, A. and Aigner, T. 1991. Storm deposition at the bed, facies, and basin scale: the geologic perspective. *In*: Einsele, G., Ricken, W. and Seilacher, A. (eds) *Cycles and Events in Stratigraphy*. Springer, 249–269.
Sheppard, T.H. 2007. Life's a beach: lessons from the Earth's rarest sedimentary rocks. *Geology Today*, **23**, 108–113, https://doi.org/10.1111/j.1365-2451.2007.00606.x
Shields, G., Edgar, K.M., Ratcliffe, K.T. and Dahl, T.W. 2022. Chemostratigraphy: using elements and isotopes to identify, interpret and correlate events in strata. *GSL Geoscience in Practice*, 101–120, https://www.geolsoc.org.uk/GIP001
Simmons, M.D., Miller, K.G., Ray, D.C., Davies, A., van Buchem, F.S.P. and Gréselle, B. 2020. Phanerozoic Eustasy. *In*: Gradstein, F.M., Ogg, J.G., Schmitz, M.D. and Ogg, G.M. (eds) *Geologic Time Scale 2020*. Elsevier, 357–400.
Siveter, D.J., Owens, R.M. and Thomas, A.T. 1989. *Silurian Field Excursions. A Geotraverse Across Wales and the Welsh Borderland*. National Museum of Wales, Geological Series, **10**.
Taylor, A.M. and Goldring, R. 1993. Description and analysis of bioturbation and ichnofabric. *Journal of the Geological Society, London*, **150**, 141–148, https://doi.org/10.1144/gsjgs.150.1.0141
Thomas, H.H. 1911. The Skomer Volcanic Series (Pembrokeshire). *Quarterly Journal of the Geological Society of London*, **67**, 175–214, https://doi.org/10.1144/GSL.JGS.1911.067.01-04.07
Trotter, J.A., Williams, I.S., Barnes, C.R., Männik, P. and Simpson, A. 2016. New conodont $\delta^{18}O$ records of Silurian climate change: implications for environmental and biological events. *Palaeogeography, Palaeoclimatology, Palaeoecology*, **443**, 34–48, https://doi.org/10.1016/j.palaeo.2015.11.011
Tucker, R.D. and McKerrow, W.S. 1995. Early Paleozoic chronology: a review in light of new U–Pb zircon ages from Newfoundland and Britain. *Canadian Journal of Earth Sciences*, **32**, 368–379, https://doi.org/10.1139/e95-032
Veevers, S.J. 2006. *Sedimentological and Stratigraphical Studies in the Silurian of the Welsh Basin*. PhD thesis, University of Birmingham.
Veevers, S.J., Thomas, A.T. and Turner, P. 2007. Fan-delta sedimentation in the Silurian Coralliferous Formation of SW Wales: implications for the structure of the southern margin of the Welsh Basin. *Geological Magazine*, **144**, 319–331, https://doi.org/10.1017/S0016756806003013
Walmsley, V.G. and Bassett, M.G. 1976. Biostratigraphy and correlation of the Coralliferous Group and Gray Sandstone Group (Silurian) of Pembrokeshire, Wales. *Proceedings of the Geologists' Association*, **87**, 191–220, https://doi.org/10.1016/S0016-7878(76)80011-9
Woodcock, N.H., Butler, A.J., Davies, J.R. and Waters, R.A. 1996. Sequence stratigraphical analysis of late Ordovician and early Silurian depositional systems in the Welsh Basin: a critical assessment. *Geological Society, London, Special Publications*, **103**, 197–208, https://doi.org/10.1144/GSL.SP.1996.103.01.11

Xie, X. and Heller, P.L. 2009. Plate tectonics and basin subsidence history. *Geological Society of America Bulletin*, **121**, 55–64, https://doi.org/10.1130/B26398.1

Zalasiewicz, J.A., Taylor, L., Rushton, A.W.A., Loydell, D.K., Rickards, R.B. and Williams, M. 2009. Graptolites in British stratigraphy. *Geological Magazine*, **146**, 785–850, https://doi.org/10.1017/S0016756809990434

Ziegler, A.M., Cocks, L.R.M. and McKerrow, W.S. 1968. The Llandovery transgression of the Welsh Borderland. *Palaeontology*, **11**, 736–782.

Ziegler, A.M., McKerrow, W.S., Burne, R.V. and Baker, P.E. 1969. Correlation and environmental setting of the Skomer Volcanic Group, Pembrokeshire. *Proceedings of the Geologists' Association*, **80**, 409–439, https://doi.org/10.1016/S0016-7878(69)80031-3